A study on the reflective properties of Tyvek in air and underwater

Alvaro Chavarria

Department of Physics

Duke University

Date: ______________________________

Approved:

____
Prof. Kate Scholberg, Supervisor

____
Prof. Seog Oh

____
Prof. Haiyan Gao

____
Prof. Chris Walter

Submitted in partial fulfillment of the requirements for graduation with distinction in the Department of Physics of Trinity College, Duke University.

May 8, 2007

Abstract

Tyvek is a material that is used extensively in the outer detector of the Super-Kamiokande neutrino observatory. The Monte Carlo simulation of Super-Kamiokande has several routines that simulate the reflection of photons from the Tyvek. We have devised and built an experiment to measure the reflectivity of Tyvek in air and underwater on the plane of the incident light. The results from this experiment can be used to improve the Monte Carlo simulation of Super-K.

It was found that the results in air fit very well the expected function, which is a combination of Lambert's Cosine Law (due to highly diffusive reflection) and a diffused specular component that still retains some angular dependence. The results in water also agree well with the fits for angles of incidence smaller than 40°, while at larger angles of incidence the fit seems to miss the tail of the data.

The reflectivity of Tyvek in the plane of the incident light seems to be much larger in water than in air (by a factor of 2.0-2.5, depending on the angle of incidence). This is consistent with the fact that, in water, the reflectivity functions appear to have a predominant diffused specular component.

The current implementation of the reflection of photons from Tyvek in the Monte Carlo does not agree well with the experimental results. In the simulation, the number of photons that reflect according to Lambert's Cosine Law is too large compared to the number that reflect in a diffused specular fashion. This leads to large disagreements with the data, especially for results at large angles of incidence and in water, where the diffused specular component dominates.

Contents

1 Introduction

Super-Kamiokande is a large, cylindrical water tank (40 m $\times$ 40 m) located in a mine 1 km underground near the town of Kamioka, Japan [1]. Super-K is a water Cherenkov detector designed to study neutrinos. It detects charged particles by measuring the light that is produced as these particles exceed the speed of light in water (c/1.33) and produce a shock wave. Photomultiplier tubes (PMTs) are located both in the inner walls (looking in) and the outer walls (looking out) of the cylinder and detect the blue and ultra-violet light (part of the spectrum of Cherenkov radiation) as it is incident on the walls of the tank. The outer looking PMTs are part of Super-Kamiokande's outer detector (OD). This detector serves mostly as a veto to tell when a particle goes in or out of the tank. This is useful because it allows us to tell when a charged particle that is detected by the inner detector (ID) was created by some interaction in the ID or it came from the outside. Additionally, the outer detector is useful for neutrino detection as the information it provides is of great importance for partially-contained neutrino events and for studies on upward-going muons.

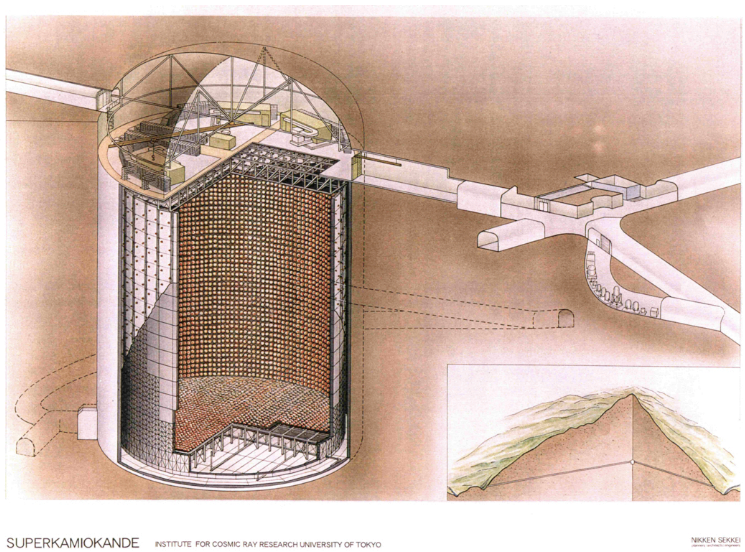

Figure 1: Picture of the Super-Kamiokande neutrino observatory [2].

Given that the OD serves mostly as a veto, it is important to collect as much light as possible in order to be able to veto particles over a larger energy range. Thus, a cheap and easy solution that will increase the light collection in the OD is necessary. Enter Tyvek.

1.1 Tyvek and its properties

Tyvek is a paper-like material made with continuous, very fine, randomly distributed and nondirectional fibers of high-density polyethylene. According to its manufacturer, DuPont, Tyvek "offers all the best characteristics of paper, film and fabric in one material... [Tyvek is] lightweight yet strong; vapor-permeable, yet water-, chemical-, puncture-, tear- and abrasion-resistant. Tyvek is also low linting, smooth and opaque." [3]

Also, according to DuPont, Tyvek is remarkably flexible and its dimensions are negligibly affected by humidity and temperature. It has a neutral pH and, not only does it not absorb water, but its "physical properties are not affected by water."
Studies have been conducted on the transmittivity of Tyvek [4], and the results have been found to be consistent with DuPont's value for the opacity of Tyvek, which is 92%. In the Product Handbook, DuPont states that Tyvek returns a higher result in the GE Brightness test [5] than a pure titanium

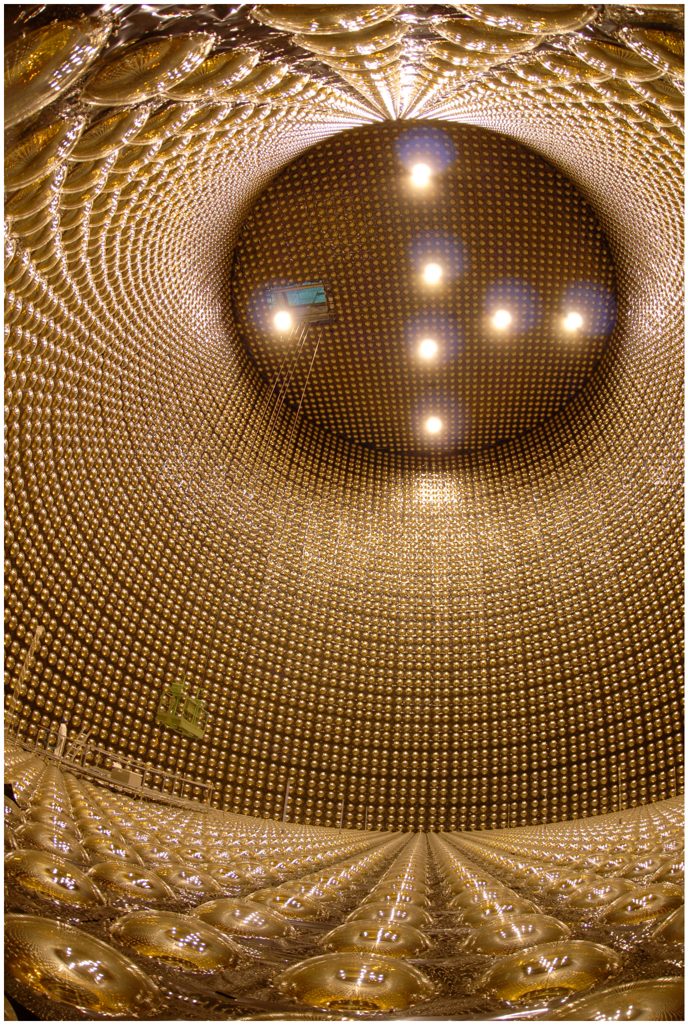

Figure 2: Photograph of Super-Kamiokande's inner detector [2].

Figure 3: A sheet of Tyvek.

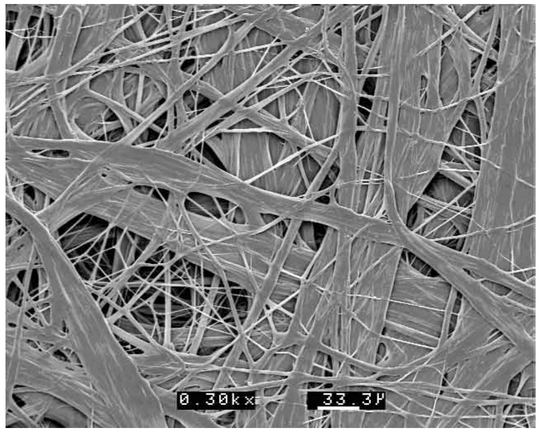

Figure 4: Electron microscope photograph of Tyvek [6].

dioxide pellet (94.1 vs. 93.8). In addition, color values for Tyvek are L=97.8 (100 for perfect white), a=0.3 green component, b=0.1 yellow component, w=96.5 overall color acceptance [7].
The reflective properties of Tyvek have also been previously studied [8],[9].

1.2 Uses and applications of Tyvek

Tyvek has been used extensively in many industries. It has been used for protective apparel (jump suits), envelopes, medical packaging, covers and in the construction and graphic industries. Most importantly, though, Tyvek has been used in some particle detectors, e.g. the Super-Kamiokande neutrino observatory in Japan.

1.2.1 Tyvek in Super-Kamiokande

Its permeability, high reflectivity and light scattering properties make Tyvek a good material to be used in the OD. Tyvek is placed in between and in front of the PMTs. This way, Cherenkov light that is created in the outer detector will reflect off and be scattered multiple times by the Tyvek, increasing the path length for a photon in the OD and, thus, increasing its likelihood to be detected by a PMT. Also, Tyvek is used to segment different parts of the outer detector (i.e. prevent light from going from one segment to another). This is possible due to the high opacity of Tyvek.
The water used in Super-K is ultra pure in order to increase the path length of photons in water. Thus, it is advantageous for Tyvek to be pH neutral so that it does not contaminate the water.
Figure 7 shows a charged particle coming from the outside (could be a cosmic ray) that pokes through the top and goes into the inner detector. Figure 8 shows how such an event would look like in Super-K's event display. The event display shows an unfolded picture of the inner and outer surfaces of the detector (the inner detector is the large surface and the outer detector is the smaller surface on the top-right). The colors represent the quantity of charge output by the PMTs (red being the highest), which should be proportional to the number of photons incident on the PMTs. As it can be seen, there is some light collected at the top and bottom of the outer detector, which means that the particle entered the tank from the top and exited at the bottom and, therefore, it can be successfully vetoed. The light collection in the outer detector is increased by the use of Tyvek.

The Super-Kamiokande collaboration has a GEANT3-based Monte Carlo simulation of the detector. Photons are tracked in the OD as they bounce off the Tyvek. A function has been programmed to simulate how the photons reflect from the Tyvek. The more realistic this simulation is, the closer the agreement between the Monte Carlo and the data. A good agreement is desirable, as it helps us understand better what Super-K's output looks like when charged particles travel in the outer detector. To work as a veto, a good accuracy in the reflectivity of Tyvek is not absolutely necessary, but a more

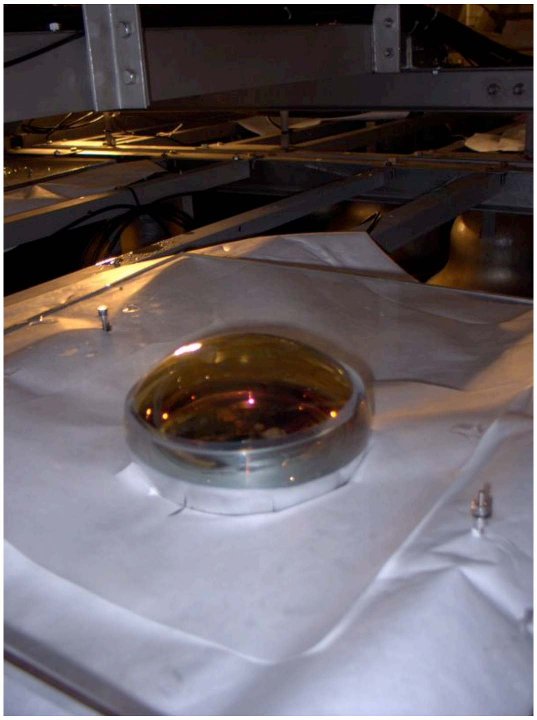

Figure 5: A photomultiplier tube in Super-K's OD. Notice the surrounding Tyvek [10].

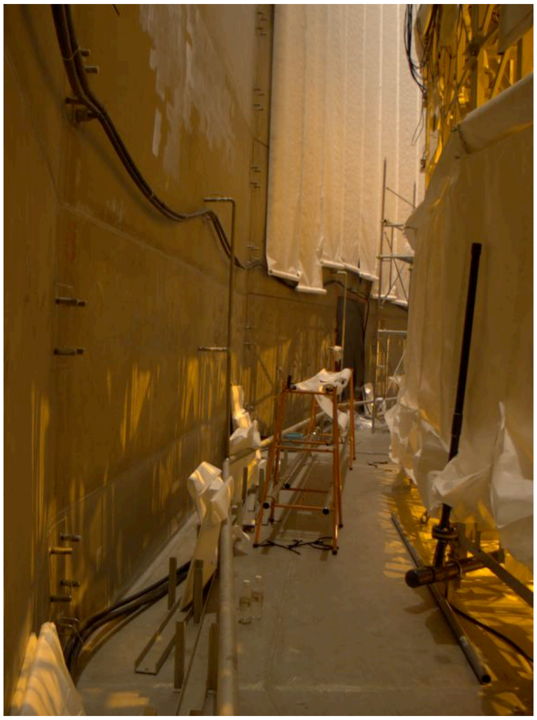

Figure 6: Tyvek being installed in the OD [10].

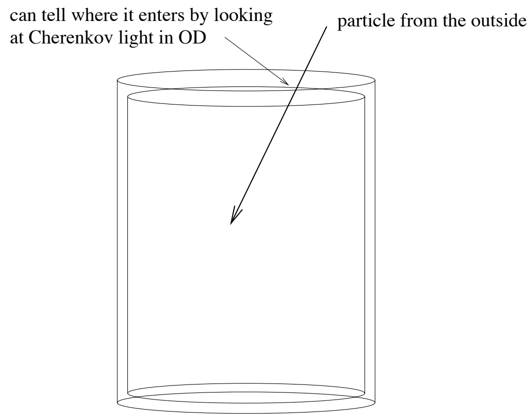

Figure 7: Diagram showing a charged particle going into the detector.

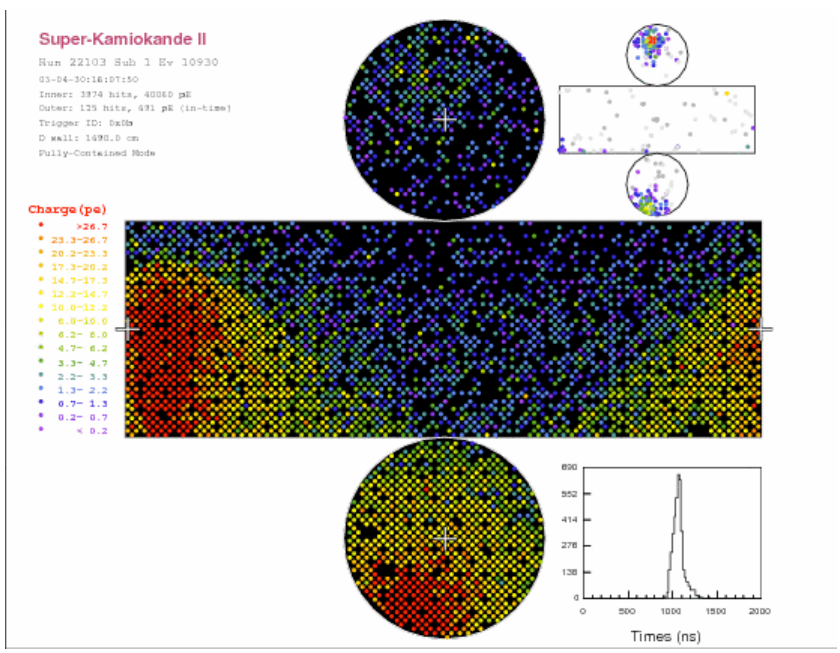

Figure 8: Super Kamiokande's event display showing a particle entering from the top of the tank.

realistic implementation of the reflective properties of Tyvek might help us better understand partially contained events, i.e. neutrino interactions whose reaction products create some light in the OD (these may be highly energetic muon neutrinos, etc.), and other phenomena for which the outer-detector provides valuable information, like studies on ultra-high energy upward-going muons.
Thus, we have devised an experiment to measure the reflective properties of Tyvek. The results will be used to evaluate, and later to improve, the current simulation of the reflection of photons from Tyvek in Super-K's Monte Carlo.

1.3 A first look at the reflective properties of Tyvek

It can be noticed from the properties of Tyvek (or just by taking a look at a piece of it) that it is remarkably white and that it has a very high opacity. This does not only mean that Tyvek reflects most of the light (of all visible frequencies) that is incident on it but also that, at the microscopic level, the fibers of Tyvek scatter the light sufficiently so that it comes out with a high degree of uniformity. This seems plausible as photons can reflect and refract from multiple microscopic fibers in the Tyvek before being reflected off the surface. A flat piece of material that reflects light in a diffuse fashion obeys **Lambert's cosine law**.

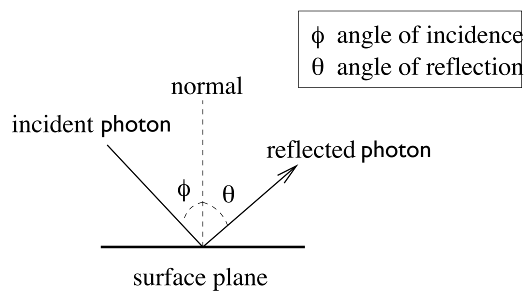

Figure 9: Diagram showing a photon reflected of the surface of the Tyvek.

1.3.1 Lambert's Cosine Law

Suppose a small area dS of material that reflects light in such a way that the number of photons per unit time per unit projected area that the surface emits is the same in all directions. Thus, let us define B as a constant, which is the number of photons emitted per unit time per unit projected area per unit solid angle. Consequently, the number of photons per unit time (i.e. the radiant flux, Φ) that fall within an element solid angle will be

$$d\Phi = BdS_{proj}d\Omega \tag{1}$$

$$d\Phi = B\cos\theta dSd\Omega \tag{2}$$

where θ is the angle between the normal of the surface and the direction vector to the solid angle element. $dS_{proj} = \cos\theta dS$ is the area element as seen from the solid angle element (its projection).
Assuming that the light is being measured sufficiently far away from the surface (r is large), and the area of the piece of reflective material is sufficiently small (S), we may approximate $S = dS$. Furthermore, if the light is being collected over a small enough area, A, such that A/r^2 is small, then the solid angle covered by the detector can be approximated to be the element solid angle. Therefore, we may write

$$\Phi = \frac{BAS}{r^2}\cos\theta \tag{3}$$

$$\Phi(\theta) = \Phi_o\cos\theta \tag{4}$$

where Φ is the flux of the light (number of photons per unit time) measured at angle θ and Φ_o is Φ for $\theta = 0$. [11]
This is Lambert's Cosine Law.

A closer look at Tyvek reveals that the material may not reflect light in a perfectly Lambertian fashion. By shining a laser pointer on Tyvek it is possible to see that some of the light is reflected from the Tyvek in a preferred direction dependent on the direction of the incident light, very much like headlights reflecting from the asphalt. Clearly, it is not possible to see one's face while staring at Tyvek, which suggests that this component is relatively small, yet it might be an important characteristic of the reflectivity of Tyvek.
Some photons may be specularly reflected from the surface of the surface fibers straight back into the medium (as opposed to being refracted and scattered within the material). Still, due to the irregular surface of the Tyvek we still expect these photons to be somewhat scattered and, therefore, some diffused specular reflection is expected from the Tyvek.

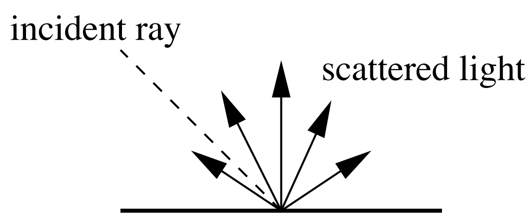

Figure 10: Diagram representing lambertian reflection.

1.3.2 Diffused specular reflection

Diffuse specular reflection is the name given to reflection of light from irregular surfaces, like Tyvek. The photons reflect from the surface obeying the law of reflection but, due to the random orientations of the surface, the reflected light has some scattering i.e. a light beam that is incident at angle ϕ will reflect over a range of angles of reflection around $\theta = -\phi$ depending on how irregular the surface of the reflective material is.
This diffuse reflection can be modeled on the plane of the incident light by supposing that the reflected photons have a gaussian distribution in the angles of reflection centered at the angle of specular reflection. Thus, we may write for a ray of light with an angle of incidence ϕ,

$$\Phi(\theta, \phi) = Ce^{-(\theta+\phi)^2/s} \tag{5}$$

where Φ is the flux of the light measured by a detector that covers a small solid angle, θ is the angle between the normal of the reflective surface and the position of the detector on the plane of the incident light, C is a constant such that integrating Φ over all angles is equal to the total intensity of the incident light beam and s is the spread of the gaussian, which is related to the irregularity of the surface of the material.

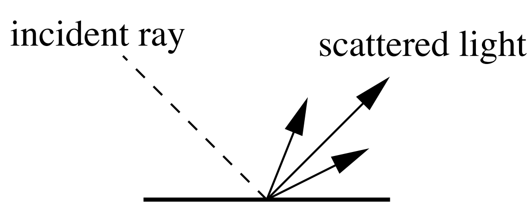

Figure 11: Diagram representing diffused specular reflection.

It is expected, from initial inspection and knowledge of the inner structure of Tyvek, that its reflective characteristics manifest both lambertian and diffused specular reflection. Thus, we predict that the flux of light reflected by Tyvek as measured by a detector at θ on the plane of the incident light, for a fixed angle of incidence ϕ, to be of the form

$$\Phi(\theta,\phi) = C_1' e^{-(\theta+\phi)^2/s} + C_2' \cos\theta \tag{6}$$

where C_1', C_2' are constants with respect to θ that are related to the contributions from each mode of reflection. Like s, these could depend on ϕ.
If the detector subtends the same solid angle at all positions, then the previous expression is proportional to reflected intensity, I, which is the fraction of the incident light that is reflected at a particular angle per steradian

$$I(\theta,\phi) = C_1 e^{-(\theta+\phi)^2/s} + C_2 \cos\theta \tag{7}$$

We can compare this to the current reflectivity function in the Monte Carlo, which is dependent on both the angle of incidence and the angle of reflection of the incident photon. It is a superposition of a cosine (lambertian), gaussian (diffused specular) and uniform (isotropic) functions. This function on the plane of the direction of the incident photon is

$$I(\theta,\phi) = N\left(0.425F(1-G(\phi))\cos\theta + 1.83G(\phi)e^{\frac{-(\theta+\phi)^2}{15^2}} + 0.0477F\right) \tag{8}$$

where F is the fraction of the hemisphere that is covered by a detector that subtends a small, constant solid angle as it sweeps all angles of reflection and $G(\phi)$ is the array given below. Also, the parameter value `DSTYVKM`=0.85 was used (this is a parameter set in Super-K's Monte Carlo simulation).

Angle of incidence	$G(\phi)$
$0-9$	0.02
$9-18$	0.021
$18-27$	0.022
$27-36$	0.026
$36-45$	0.03
$45-54$	0.038
$54-63$	0.053
$63-72$	0.083
$72-81$	0.16
$81-90$	0.54

`DSTYVKM` is the probability that a photon is reflected in a diffused specular or lambertian fashion. Thus, `DSTYVKM` $\times G(\phi)$ is the probability that a photon will be reflected in a gaussian (i.e. diffused specular) way.
Notice that in the current simulation all photons that are reflected in a gaussian way are reflected to the plane of the direction of the incoming photon, while photons reflected in either isotropic or lambertian fashions are reflected over the entire surface of the hemisphere whose base is the plane of the Tyvek and whose radius is the distance between the Tyvek and the detector. Therefore, the factor F comes in to calculate how many of the photons that are reflected over the entire surface of the hemisphere fall within the area covered by the detector (F may be introduced only if we assume that this area is small). According to this function, as the area covered by the detector gets smaller, the number of detected photons that are reflected in lambertian and isotropic fashions decreases, but the number of detected photons from gaussian reflection remains the same. Thus, if we use a detector that sweeps a small enough area (as close to ideal as possible), then the gaussian component in the function from the Monte Carlo

will be inflated. As the plane of the incident light is an artificially 'special' plane, comparing the results from the experiment to this expression is not a fair comparison to the Monte Carlo. It is a good idea, then, to add a term to the Monte Carlo expression, H,

$$I(\theta,\phi) = N\left(0.425F(1-G(\phi))\cos\theta + 1.83HG(\phi)e^{\frac{-(\theta+\phi)^2}{15^2}} + 0.0477F\right) \tag{9}$$

and assume that the photons that are reflected in a diffused specular (gaussian) fashion are distributed symmetrically about the axis $\theta = -\phi$, over an angular range of $\pm 2\sigma = \pm 30^\circ$ above and below the plane of the incident light. H will then be the fraction of the solid angle defined by this angular range that is covered by the detector as it sweeps all angles of reflection. The addition of this term will give a better measure of how the shape, especially the relative contributions of the lambertian and diffused specular components, of the reflectivity function used in the Monte Carlo compares to the data.

2 Apparatus

2.1 Overview

To test Equation 7 it is necessary to design an experiment that measures three variables independently: i) ϕ, the angle of incidence of the incident light on the Tyvek, ii) θ, the angle at which the reflected light is being measured and iii) Φ, the flux of the light collected at angle θ.
The general idea for the experiment is the following. A laser diode beams light onto a piece of Tyvek that is held on a rotation stage (the plane of the Tyvek is perpendicular to the surface of the stage). Thus, rotation of this stage allows us to change the angle of incidence for the laser beam (ϕ). Then, an arm is attached to another rotation stage, whose center of rotation is aligned to that of the first stage. The rotation of this stage allows the arm to be moved half-a-circle (180°) about the Tyvek piece. This arm holds a piece of fiber that lies horizontally on the same plane as the laser beam and is pointing towards the Tyvek. The fiber is connected to a light detector (for example, a PMT). Thus, by rotating the second stage (i.e. changing θ) it is possible to measure Φ over the entire range of angles of reflection for a particular angle of incidence (ϕ).

2.2 The dark box

It is very important in this experiment to minimize backgrounds from external light sources; for this reason the experiment is run in a dark box. The box that is used is a light and water-tight dark gray PVC box with a lid that lays on top. In addition, the box has some holes on the side at the top to run cables and fibers into the system. After running these through, duct tape and electrical tape was used to seal the holes. Also, at the bottom of the box in one side there is a tap. The experiment can be run underwater and therefore, this tap allows us to easily drain water out of the box and control the water level.

2.3 The mechanical rotation system

The rotation stages that were selected for use in this experiment were ordered from OptoSigma (SigmaKoki SGSP-40YAW). These are motorized rotation stages that can be controlled using LabView[12]. Due to the fact that the experiment needs to be run in the dark, motorized rotation stages offer the great advantage that they can be operated externally by just running a cable into the dark box, as opposed to some complicated mechanism for manual operation. These rotation stages have full 360° range and can rotate in small steps of $1^\circ/400$.

As the experiment is run under water, it is necessary for the stages and all other electronics to remain above the water. In addition, proper alignment and good stability are crucial.
As it can be seen from Figure 14, the stages can be screwed onto a surface using three M3 screws. In order to have their centers aligned, we decided to use a $1/4''$ thick aluminium square with four M3 threaded holes centered and with the right separation such that the stages can be screwed onto the block. One of

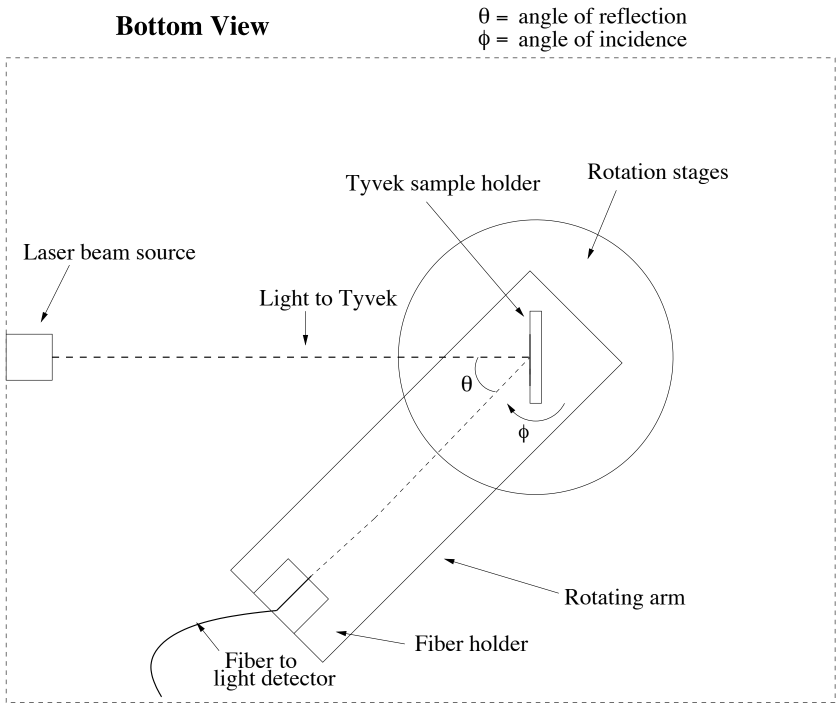

Figure 12: General diagram for the Tyvek reflectivity experiment.

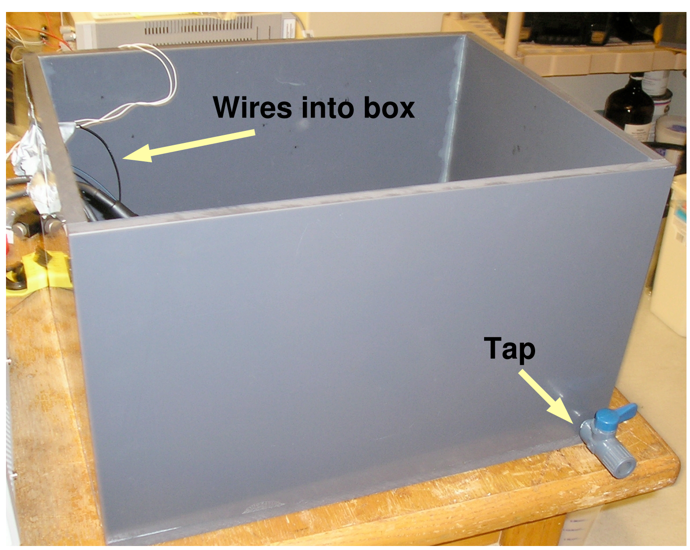

Figure 13: Photograph of the dark box.

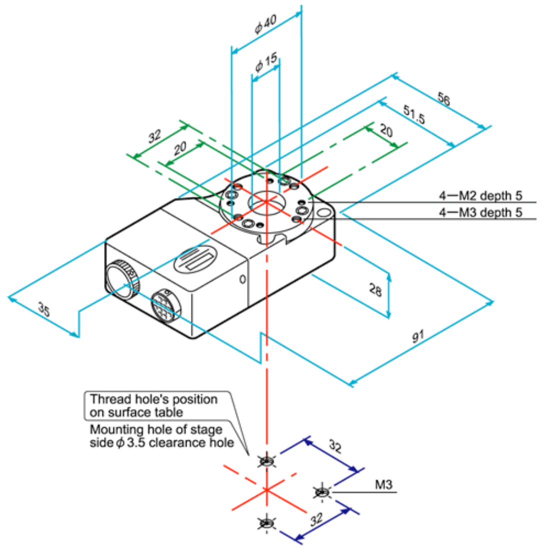

Figure 14: Diagram of SigmaKoki SGSP-40YAW.

the tables is screwed on the top of the square and the other is screwed upside-down on the bottom of the square. Because the rotation axis of the stages should be in the middle of these four holes (according to the manufacturer's specifications), then the axes of both stages should coincide.

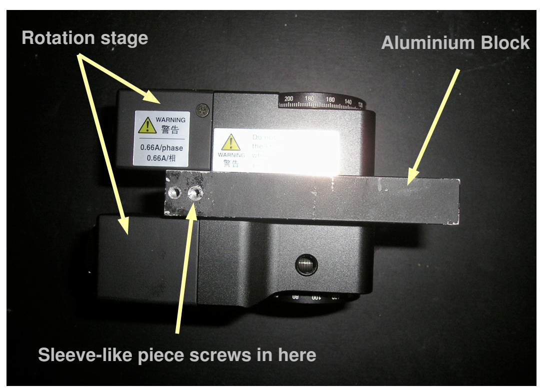

Figure 15: Photograph of the rotation stages installed on the aluminium block.

The bottom stage is the one on which the Tyvek sample is placed. To hold the plane of the Tyvek sample perpendicular to the rotation stage (i.e. parallel to its axis of rotation) a holder for this piece had to be designed. The rotation stage has four M3 threaded holes centered on the rotation axis so that a part can be screwed on the rotating table of the stage. The piece that was designed is shown in Figure 18 and Figure 19.

The base of this Tyvek holder has holes such that it can be screwed on a rotation stage. A vertical part is attached to the base such that one of its lateral faces is directly on top of the midpoint between the holes on the base, i.e. the face where the Tyvek piece is placed. A 1 mm hole runs across this piece so that a fiber can be put through it for normalization and alignment purposes. Notice that the piece is not much wider than the width of the hole. The position of this hole is where the laser beam is incident

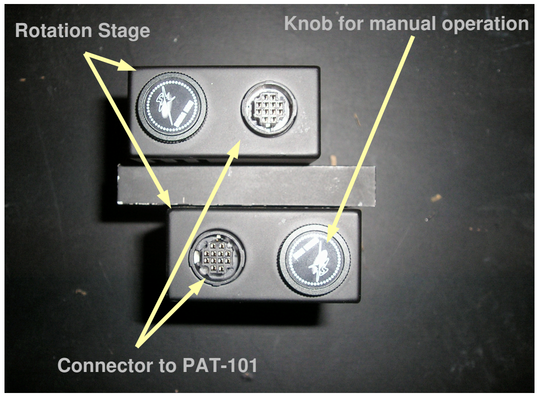

Figure 16: Photograph of the back of the rotation stages.

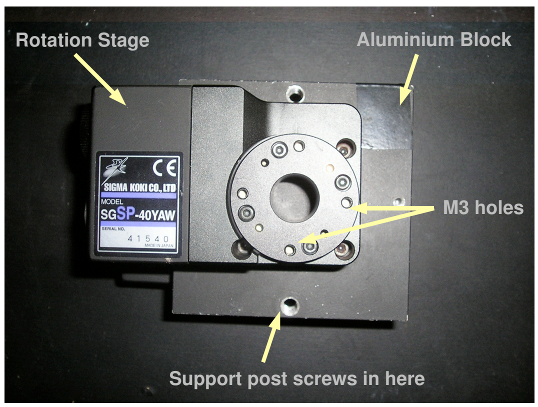

Figure 17: Photograph of the top of the rotation stages.

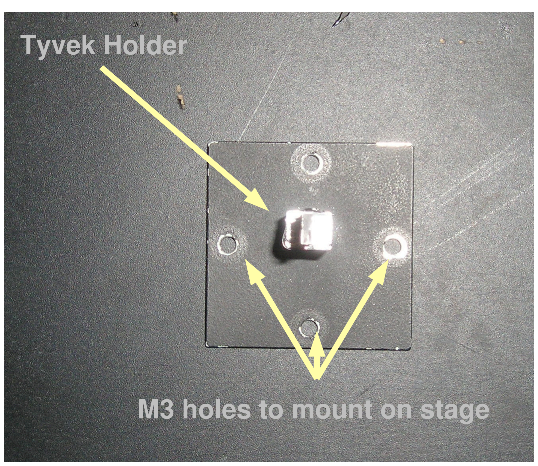

Figure 18: Photograph of the top of the Tyvek holder.

and thus, where the Tyvek sample should be placed (covering the hole).

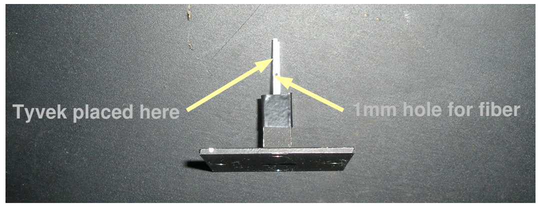

Figure 19: Photograph of the side of the Tyvek holder.

An arm has been designed to be screwed on the top rotation stage. Like the Tyvek holder, it has four M3 holes such that it can be screwed on the rotating table of the stage. This arm goes outside of the rotation stage and then it has at the end a piece that extends downward. At the end of this piece there is a small horizontal extension with a 1 mm hole that runs through it (this is where the collecting fiber will be placed). The design is such that, when assembled, the hole is at the same vertical position as the hole in the Tyvek holder and it is pointing towards the rotation axis of the stages. The distance between the face of the bottom horizontal extension and the axis of rotation is $r = (94.0 \pm 0.1)$ mm.

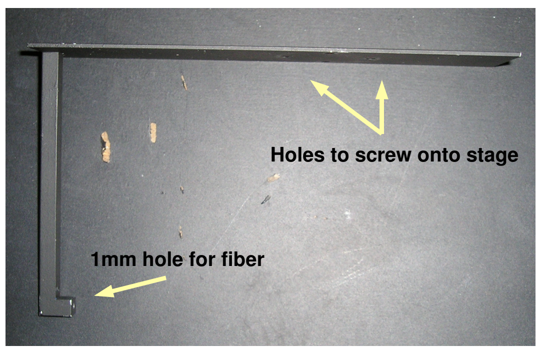

Figure 20: Photograph of the side of the arm.

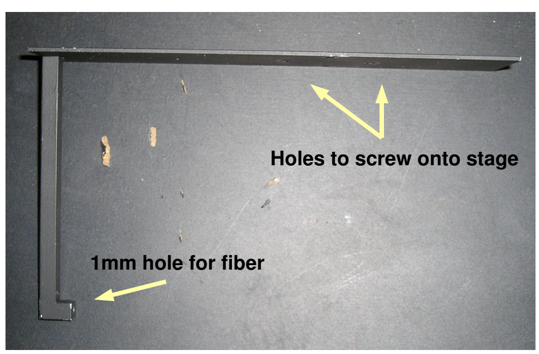

Figure 21: Photograph of the top of the arm.

The aluminium square and the stages have to be held in a stable position above the ground. To do this, the aluminium square has two threaded holes near its sides in which two optical posts can be screwed. These posts are connected to some smaller diameter posts (these pierce through the plane of the laser beam, therefore there might be some angles at which these supports block the light to the collecting fiber and thus, it is in our best interest to have these be as narrow as possible). These smaller posts are, in turn, connected to post holders that are screwed on regular posts that are held in position by post holders that are fixed on an optical table. (see Figure 22)

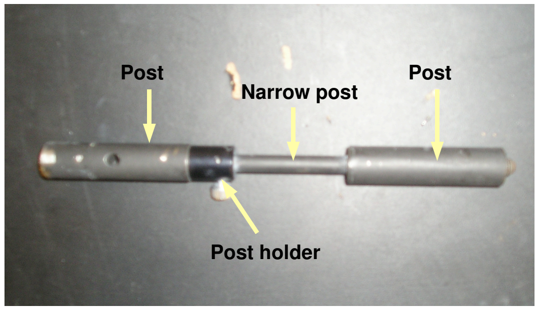

Figure 22: Photograph of one of the supports.

Finally, for further support a piece has been designed that is screwed on the aluminium block. Four screws go into threaded holes on the lateral faces of the aluminium block and hold this part in position, forming a sleeve that barely allows the bottom rotation stage in. This additional piece has a threaded hole in its center (Figure 25) that lies under the bottom rotation stage when assembled. This way, a post can be screwed under the bottom rotation stage, behind the Tyvek holder. This post can be then placed in a post holder that is screwed on the optical table, offering extra support if necessary.

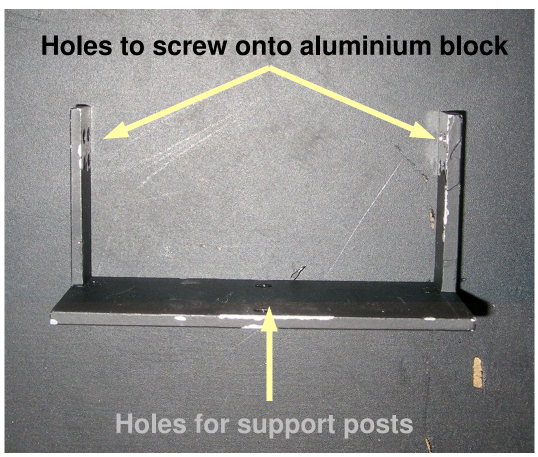

Figure 23: Photograph of the sleeve-like piece.

To minimize backgrounds it is of great importance to keep the reflection of light inside the box to a minimum and thus, all the custom made aluminium parts are spray-painted black.
A picture showing the mechanical rotation system in its full glory follows. (Figure 26)

2.4 Controlling the rotation stages using LabView

As it has been said, the OptoSigma motorized rotation stages can be controlled remotely. Each rotation stage is connected to a controller (PAT-101) via some propietary connector. These controllers connect

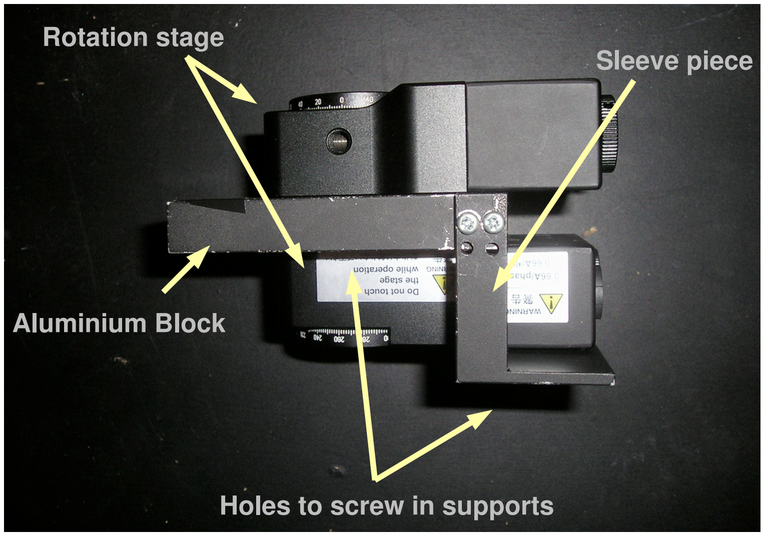

Figure 24: Photograph after installation of sleeve-like piece.

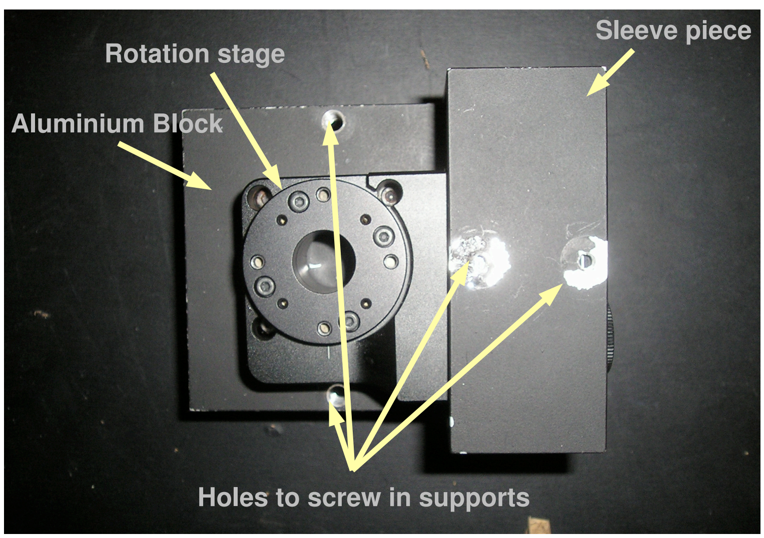

Figure 25: Bottom photograph after installation of sleeve-like piece.

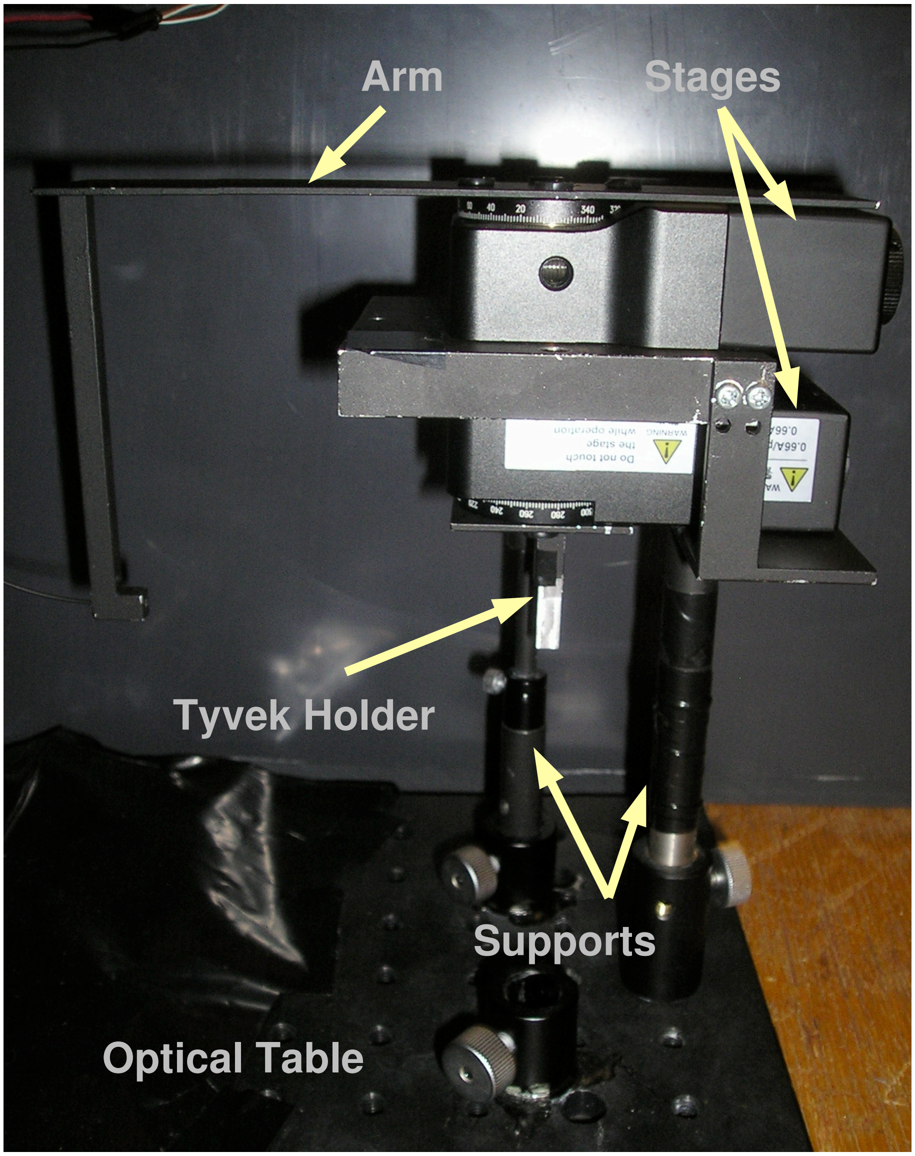

Figure 26: Diagram of the assembled mechanical rotation system.

to the serial ports of the computer.
Software was installed and setup such that the PC can communicate to the rotation stages. This software includes LabView functions like `Move` and `Origin` that can be used to operate the stages.
The `Origin` function moves the stage to the 0° position and sets it accurately at the origin. The `Move` function rotates the stage a particular number of steps (400 steps in 1°) either clockwise or anticlockwise.

2.5 Light collection

In this experiment, 0.5 mm diameter jacketed optical fibers (1 mm diameter including jacket) are used. The fiber carries the light to the light detector. In this experiment, the light detector used is a photomultiplier module (PMT) (Hamamatsu HC124-02). This module has its own high voltage power supply, therefore, for operation, it needs to be supplied with ± 12 V and a control voltage between 0 and 1.2 V. This control voltage is proportional to the internal high voltage and therefore, this sets the gain of the PMT. The output of the PMT is a DC potential difference between an output terminal and the ground terminal.

Figure 27: Photograph of two Hamamatsu HC124-02.

In the current setup, the PMT is connected to a power source that supplies the ± 12 V. Its control voltage is set by a second power supply that has two independent outputs (Agilent E3620A).

2.5.1 Stability of PMT

Before making any light flux measurement using a PMT it was necessary to check if the PMT output is constant when a constant flux of light is shone on the photocathode. To do this, we set a green light emitting diode (LED) with a constant current through it. The flux of the light emitted by the LED should be proportional to the current. In case the LED had some transient behavior, we left it on for a few hours. Then, we turned the PMT on for a few hours with the CV set to 0.5 V and, using an ammeter, we measured the output of the PMT (in this case the current was measured as opposed to the potential difference; this is acceptable as both values should be proportional to each other according to Ohm's law).

Figure 28 shows the PMT output with respect to time for different light intensities (LED currents). As it can be seen, for output currents greater than 60 mA, it takes a few minutes for the PMT output to settle. Assuming that the LED current is approximately proportional to the flux of the light it emits (this is one of their known properties), then the small separation between the 4.0 mA and 3.0 mA curves suggests that, at this level, the PMT is relatively close to its saturation range (where the output is no longer linear). Thus, if our experiment is run away from saturation (which corresponds to $\approx$11 V output), then the PMT should be stable.

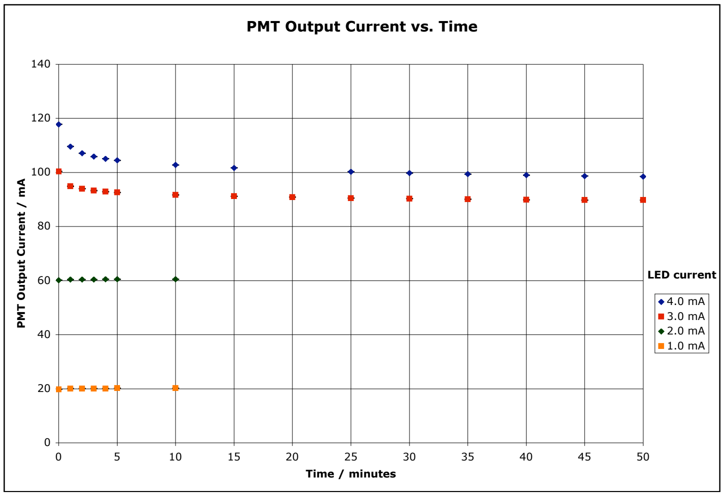

Figure 28: Stability of Hamamatsu HC124-02.

2.5.2 Linearity of PMT

It is important to check the linearity of the PMT. If we intend to accurately measure the flux of the light that is collected by the fiber, then it is desirable for the output voltage of the PMT to be linearly dependent on the flux of the collected light. To check this, we decided to run a test using some neutral density filters (Edmund Optics 55222). In this setup, the PMT was placed inside a dark box and a green LED was placed near it inside a cardboard box with an open hole. The HV control voltage (CV) was set to 0.6 V and the current through the LED was kept constant. The PMT output (in V) was measured. Then, neutral density filters of increasing optical densities were placed covering the hole, decreasing the flux of the light that reaches the PMT. Measurements were made after each filter was in place. The optical densities of the filters are 0.15, 0.3, 0.4, 0.6, 0.9 and 2.5. The results are given in Figure 29, where the flux is normalized by setting the flux with no filter to 1.

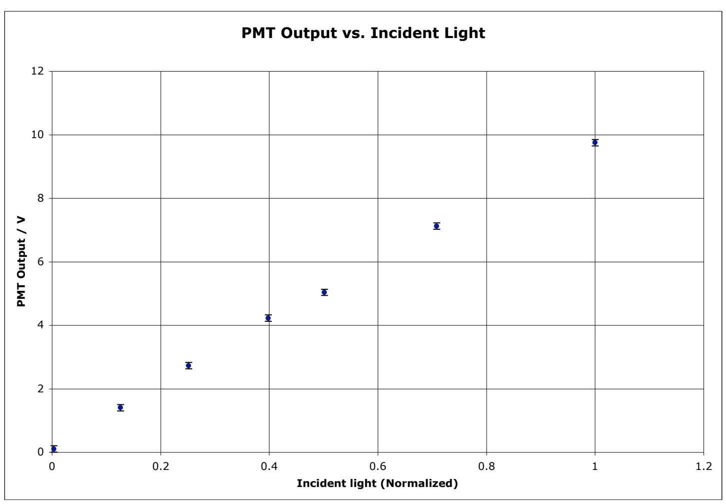

Figure 29: Linearity of Hamamatsu HC124-02.

As it can be seen, the DC measurement of the potential difference across the PMT output terminals is proportional to the flux of the incident light on the photocathode. This relationship holds to at least 10 V of PMT output.

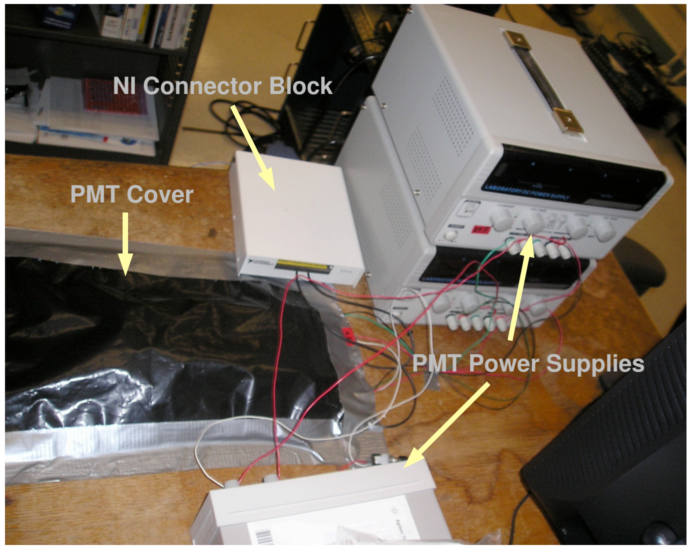

Figure 30: Photograph of power supplies and PMT cover.

2.6 Data Acquisition (DAQ)

When the experiment is run, the PMT output is measured using LabView. To do this, a connector block had to be bought (National Instruments SCB-68) that connects to a PCI card (National Instruments PCI-6221) in the computer. This interface allows the precise measurement of potential differences between terminals that are connected to the input box.

In this experiment, the output terminals of the PMT are connected to separate inputs in the box. After proper installation, a `DAQ Assistant` function was created in a LabView program and the system was setup to take DC Voltage measurements from the PMT outputs.

Settings had to be found such that the measurement adequately represents the intensity of the light incident on the PMT. It was noticed that if seen at high enough resolution (1 ms time window), the output of the PMT is very jumpy, even with a stable light source like the LED. So, in order to obtain a constant output for a constant intensity light source, some averaging had to be done. The final settings that were used, which seem to give a stable PMT output, is a DC average of $5{\times}10^5$ samples that are taken at a rate of 100 kHz (i.e. a measurement every 10 μs).

2.7 The laser mechanism

A system had to be developed so that light can be beamed onto the Tyvek sample. The laser that was used in this experiment is a green (532 nm) laser diode manufactured by LaserMate (Model No. GMP-532-XF3-CP). This laser is supplied 3V (as specified by the manufacturer) by a bench top DC power supply. The color of the Cherenkov light that is detected in Super-Kamiokande is blue and ultraviolet, but blue/UV lasers are too expensive and therefore, we chose the lowest frequency laser within our budget.

To be able to do the experiment underwater we decided to have the laser beam go initially downward, such that the diode can be out of the water and the light can enter perpendicular to the surface. Then, underwater, we have a mirror at a 45° angle, so that the beam can be reflected to the plane that is perpendicular to the surface of the Tyvek sample.

This part of the setup is mounted on a manual z-translation stage by Edmund Optics (Part No. 55024).

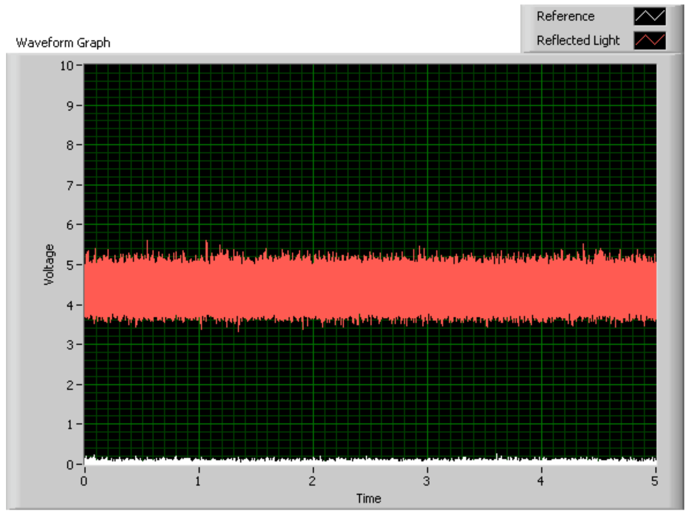

Figure 31: PMT output in the LabView screen. 5 s time window and measurements every 10 μs.

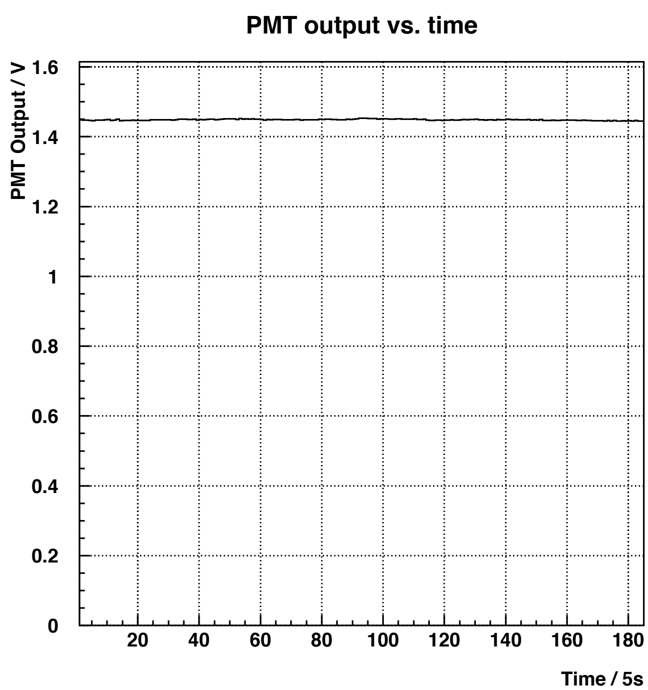

Figure 32: PMT output if averaged over 5 s.

This allows us to move the mirror up and down and thus, the plane of the beam can be raised and lowered for easier alignment. The mirror (Edmund Optics 43853) was glued using epoxy to a part that has a 45° face (Edmund Optics 54011) that screws into a post that is held vertically by the translation stage.
A large block of aluminium with a hole through it and a screw is used to hold the laser in place. This block also serves as a heat sink. This block is glued to the top of the translation stage such that the hole is vertical and, when the laser is in place, the beam goes straight down and reflects off the mirror. A photograph for the entire mechanism follows. (Figure 33)

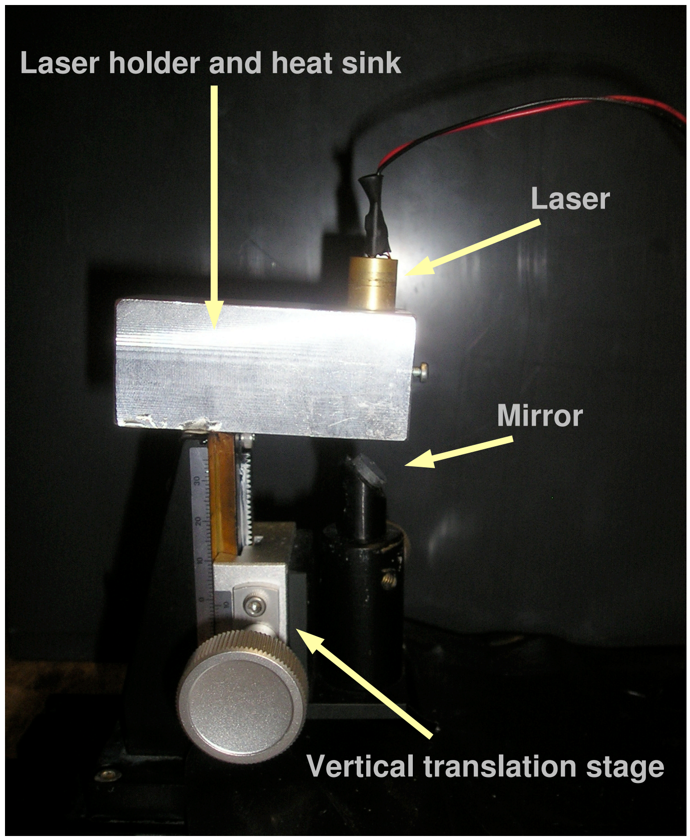

Figure 33: Photograph from the side of the laser mechanism.

2.7.1 Laser output power stability

For this experiment it is important to have a constant flux of incident light. Thus, it is necessary to know the output power characteristics of the laser. The manufacturer of the laser claims that the variations in the flux of the beam are within ±2%. This was checked using the PMT.
The experiment was done using the setup for the reflectivity measurement. The laser was installed in its heat sink and it was aimed at the Tyvek. The arm was set to a position of 10°. The PMT CV was set to 0.7 V and both the PMT and the laser had been on for a few hours. The PMT output was measured every second using LabView. Data was collected for 44 hours. Two 5.5 hour segments of this long run are shown. (Figure 35 and Figure 36)

As it can be seen, there seems to be a very slight, constant decrease in output in both segments of about 0.01V/hour. Given that our reflectivity measurements should take about one hour, this should

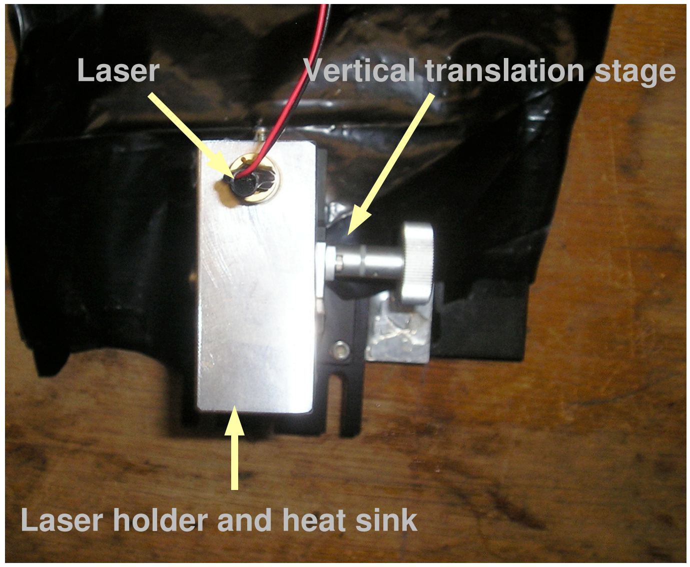

Figure 34: Photograph from the top of the laser mechanism.

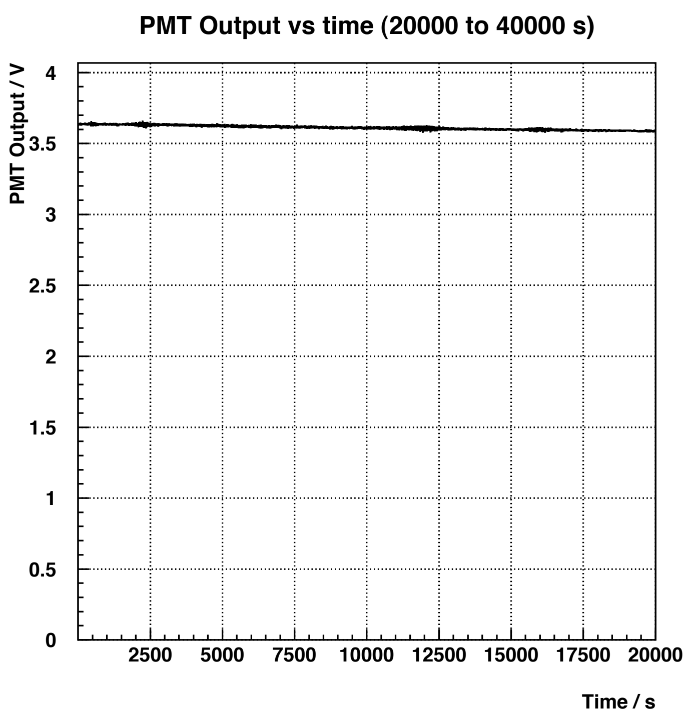

Figure 35: Segment 1 of 44 hour run to check laser stability.

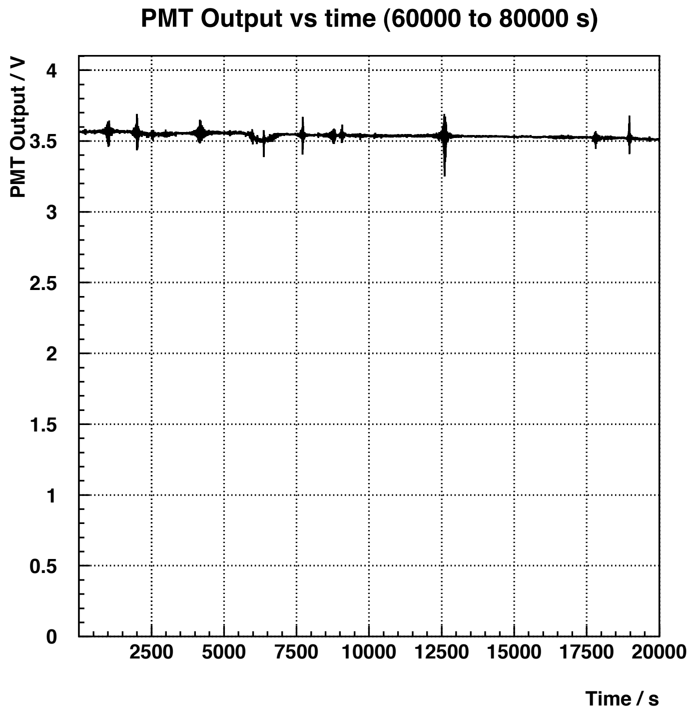

Figure 36: Segment 2 of 44 hour run to check laser stability.

not be a problem.
Something that was noticed though, was that, for some periods, the laser output is very constant, while for others there is some instability. There is no clear pattern for when these instabilities occur. Segment 1, from 20000 s to 40000 s, shows a very smooth, constant PMT output, while Segment 2, from 60000 s to 80000 s, shows some instabilities of up to $\pm 7\%$, even though most of the instabilities are smaller than that (only a few percent). The width of the spikes in Segment 2 is ≈ 30 s (these look wider due to the scale of the plot as the line width is greater than 30 s).
The stability of the laser seems to vary greatly with respect to time. Still, for most of the time, it is within the $\pm 2\%$ specified by the manufacturer.

3 Method

3.1 Alignment and setup

The entire system was setup on a black (anodized aluminium) optical board. The mechanical rotation system was placed in one end of the board while the laser and its mechanism was placed at the other end. The central support of the rotation mechanism was screwed onto the optical board while the other two supports were set on the board but not fixed, such that the structure could be rotated during alignment using the center post as pivot.
The laser was aimed at the Tyvek holder and the horizontal laser beam was moved upward using the translation stage until the laser dot was at the same height as the fiber hole in the Tyvek holder. This hole is at the same height as the hole in the arm that holds the fiber. Therefore, this can be checked by moving the arm in front of the laser beam and seeing where it hits the arm. Indeed, it was found that both holes are at the same height. (Notice that, in the first attempts, it was discovered that the laser dot had to move further up than the translation stage would allow. To fix this, the entire laser mechanism was placed on a $0.25''$ thick aluminium slab that was later covered with black plastic)

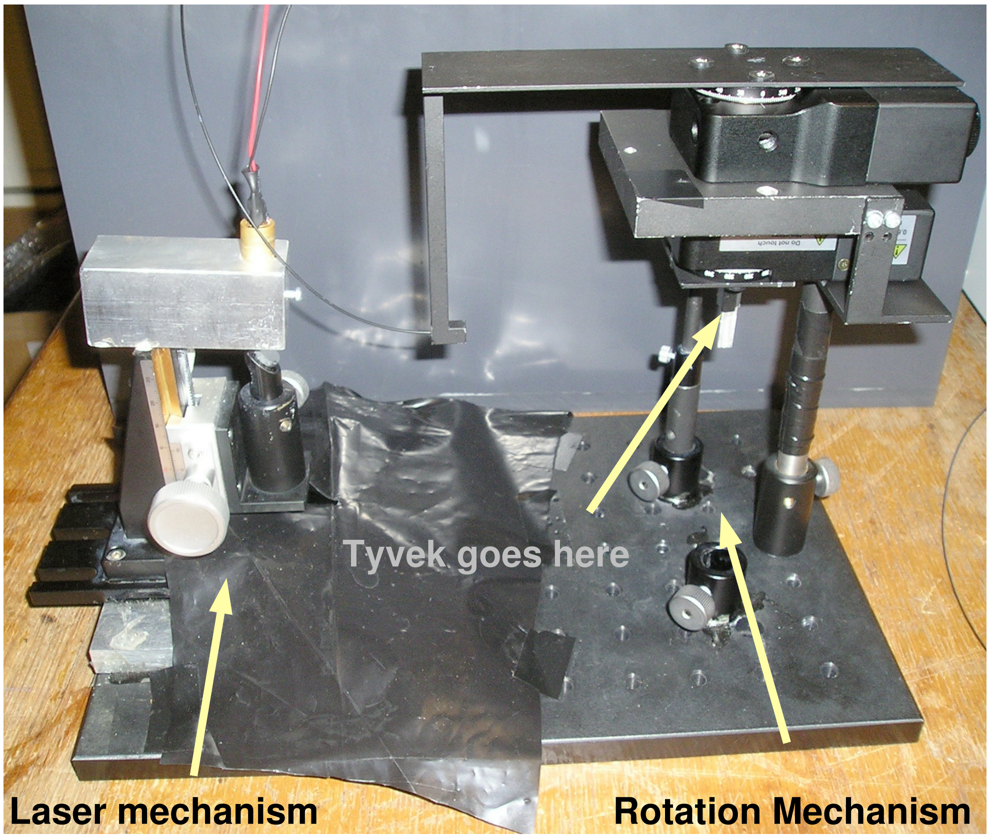

Figure 37: Photograph of the apparatus that is installed inside the dark box.

The next step was to make sure that the laser is normal to the Tyvek holder when the angle of incidence is 0°. To set this, the Tyvek holder was brought to its origin position, then a mirror was placed on the Tyvek holder such that the face of the mirror was parallel to the face of the Tyvek holder. Then, the translation stage was moved on the optical table until the outgoing laser dot on the 45° mirror was as close as possible to the incoming dot reflected from the mirror on the Tyvek holder. It was not possible to get the dots to be exactly on top of each other; in the end, there was some vertical distance between the two. This means that the laser beam and the lateral face of the Tyvek holder are not perfectly perpendicular to each other; something is slightly inclined. Because both the structure holding the rotation stages and the laser mechanism cannot be easily, carefully inclined to fix this problem, we take note of this error. The vertical distance between the two dots was $0.25''$ and the distance between the 45° mirror and the Tyvek holder is $\approx 6.5''$, thus the angle the laser beam makes with the plane that is perpendicular in all dimensions to the face of the Tyvek holder is $\tan^{-1}(0.25/13) = 1^\circ$. This value is small enough and therefore, we assume that the incident light is perpendicular in all dimensions to the plane of the Tyvek. One final check to the setup was to align both the hole in the Tyvek holder and the hole in the rotating arm with the laser beam. This was possible and the beam went through both holes and hit the middle of the center post. The positions of the arm and the holder should be the origin positions. From this, it was observed that the origin position of the arm is shifted 2° from the nominal origin. On closer inspection, it was observed that the rotation stages are slightly rotated with respect to each other, thus explaining this 2° shift.

3.2 2stages2

The LabView program that we wrote, which operates the rotations stages and controls all the data taking, is called `2stages2`. There are three inputs for this program: i) Start, ii) Stop, iii)Number of trials per angle, iv) Step size COM3, v)Step size COM4.

This program runs the following routine. The bottom rotation stage (the one that holds the Tyvek holder) goes to its initial position (Tyvek plane perpendicular to laser beam, i.e. angle of incidence = 0) and then rotates anticlockwise (as seen from above) the angular displacement that has been specified in the Start field. After this, the arm rotates anticlockwise to 90° with respect to the bottom rotation stage (i.e. places itself parallel to the plane of the Tyvek) and, in angular steps of Step size COM3, it rotates clockwise for 180°. At the end of each of these steps, the `DAQ Assistant` makes Number of trials per angle measurements of the PMT output and writes them to a file. After the PMT output has been recorded for angles of reflection for the Start angle of incidence, the bottom rotation stage rotates again, anticlockwise, a step of size Step Size COM4 and the arm repeats the procedure of making measurements for 180° about this particular angle of incidence. The process continues until the bottom rotation stage has reached the angle of incidence Stop.

This process allows us to measure the flux/intensity of the reflected light for a large range angles of incidence and reflection.

Notice that in the output of the program, positive angles correspond to anticlockwise positions for the bottom rotation stage, while they represent clockwise positions for the arm. Similarly for negative angles. This is simply due to the fact that the bottom stage is upside down.

3.3 Testing the stability of the system

In order to get reliable results it is very important for the light intensity measurements to be consistent, i.e. we should be able to set the apparatus to a particular set of conditions and be able to always obtain the same result. To test this, we ran `2stages2` with the options Start=0, Stop=80, Number of trials for angle=1, Step Size COM3=60 and Step Size COM4=25, a total of 15 times in air. A Tyvek piece was placed in the holder and the laser was turned on a few hours before the test. In this test, all parts, except the setting up of the piece of Tyvek on the holder and the piece of Tyvek itself, were the same as in the reflectivity measurement in air. PMT settings were also different from those in the reflectivity measurement; this should not matter as we are only checking for stability.

In between the measurements for a particular angle in two separate runs, the Tyvek holder and arm would have moved around significantly. Thus, if the output is consistent among these runs then we know that the mechanical operation of the apparatus does not affect the system in such a way that it changes the output.

3.4 Reflectivity measurement

The first step was to choose a sample of Tyvek that is hopefully representative of all Tyvek. Thus, we just randomly cut a piece from one of the Tyvek sheets that we got from Super-K and used it.
This piece of Tyvek was installed in a rectangular piece of metal (≈ 1 cm $\times$ 2 cm) to make its surface flat and sturdy. For the installation, we simply taped one side of the Tyvek piece to the metal and firmly pulled towards the other side and taped it. Most of the surface of the rectangular piece is Tyvek. The opacity of Tyvek is 92%; therefore we do not expect a significant number of photons that might go through the Tyvek, reflect from the metal and then go through the Tyvek again, mimicking reflected photons from the Tyvek.
The metallic piece was then glued to the Tyvek holder, making sure that the face of the Tyvek was parallel to the face of the Tyvek holder. Once the Tyvek was in place, the bottom stage was rotated manually and the position and size of the dot was eyeballed to make sure that everything was working properly. The size of the dot (which is ≈ 2 mm in diameter when incident perpendicular on the Tyvek) should increase as the angle of incidence is increased and the dot becomes elongated. Still, the dot should remain centered on the Tyvek. This was indeed the case.
Because of the laser dot on the Tyvek changes shape, it will not be possible at this point to compare the total reflectivity of Tyvek for different angles on incidence. This is because the total flux of incident light on the area of the Tyvek from which the fiber is collecting light is different for different angles of incidence, and we have not yet successfully developed a method to account for this. Thus, the normalization factor necessary to give a value for reflected intensity (i.e. the fraction of light reflected per unit solid angle) for a particular angle of incidence is unknown.
From this experiment, we can compare the shapes of the reflectivity functions for different angles of incidence and, assuming that the size of the dot does not change much between water and air (as it appears to be the case), we can also directly compare the reflectivity of Tyvek in water and air for the same angle of incidence. For this, we also assume that the flux lost as the light travels in water is negligible (the attenuation length of water is in the order of meters, while the distance between the fiber and the Tyvek is (94.0 ± 0.1) mm).
There might also be some doubt on how the size of the dot affects the range of angles over which photons are being detected for a particular angle of reflection. Ideally, only photons that come from the center of the dot should be collected by the fiber. But given that we do not know the angular acceptance of the fiber (i.e. the range of angles of incidence (as measured from the normal to the face of the fiber) over which photons are successfully transmitted through the fiber), we might be collecting photons that come from anywhere in the elongated dot. Supposing that light is collected from the edges of the dot, then for an angle of incidence of 80° and an angle of reflection of 0°, we could be collecting light over the range $0^\circ \pm 3.5^\circ$ (this is the largest possible error for all angles of incidence and reflection). Yet, the irradiance (flux per unit area) of the laser on the Tyvek decreases towards the edges of the dot. Thus, this decrease in irradiance and the possible decrease in the fiber's acceptance for photons coming from the edges of the elongated dot might make it reasonable to assume that most of the light comes from expected angle of reflection.

After the Tyvek piece had been installed (Figure 38), all the equipment was placed inside the dark box. The fiber was set in the arm with its face barely sticking out of the hole and the laser was uncovered (even though it had been on for a few hours already to be warmed up and stable). If the experiment was being run underwater, the box was filled up until the water level was a few centimeters above the plane of the laser beam. Then, the lid was set in place and the CV of the PMT was set to a particular value (even though the ± 12 V power supply had been on for at least a few hours for the PMTs to have warmed up).
Now, `2stages2` was run with the options Start=0, Stop=80, Number of trials for angle=1, Step Size COM3=5 and Step Size COM4=10. After the program ran, we obtained a file with reflectivity measurements for angles of incidence 0° to 80° (every 10°) and angles of reflection from -90° to 90° in steps of 5°. These settings were chosen because the angular resolution is sufficient and the time it takes for the data to be collected is not too long (there is less time for something to go wrong, which is especially important when running under water).

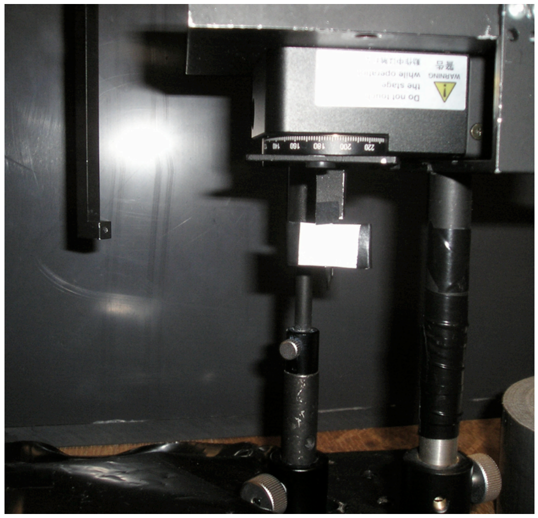

Figure 38: Photograph of the system with the Tyvek piece installed.

3.5 Backgrounds

3.5.1 External

External light backgrounds are those that are associated with light sources external to the dark box. These include the lights in the room, the sun, etc. This is the easier background to minimize as it is just a matter of properly sealing the dark box. Duct tape and electrical tape was used to seal the holes through which the cables run into the box. To make sure that most light was blocked, the lights were turned off in the room and a flash light was used to shine on the sealed areas from the outside. Then, we tried to see (with our own eyes) if light from the flash light was observable from the inside of the box. The sealing was improved until we could not tell from the inside if the flashlight was on or off.
A test was run to make sure that the external backgrounds (dark noise) had been decreased enough. The dark box was covered with the lid and the laser was turned off (i.e. there were no light sources inside the box). Then, the output of the PMT (with CV=0.7 V) was monitored as we switched on and off the lights in the room. The results are shown in Figure 39.

It is possible to see how the output jumps up and down as the lights are turned on and off in the room. The change in output is only of a few mV, which is negligible when compared to the output that is measured from the laser, which is in the order of V i.e. 1000 times larger. (The PMT output is negative because, as a matter of fact, it has been found that the output of the PMT when no light is incident on it is a few mV below 0 V, a negative pedestal, due to a DC offset, which is also negligible).

3.5.2 Internal

Internal backgrounds refer to all the laser light that is collected by the fiber that does not come from the Tyvek. This includes scattered laser light that reflects from different parts of the apparatus.
Internal backgrounds are very hard to deal with. If we could place a perfect light absorber right where the Tyvek is, such that it absorbs all the light incident on it, we could then run the reflectivity experiment and measure how much of the light comes from the internal backgrounds. Sadly, there is no such thing as a perfect light absorber and attempting this with any other material would only lead us to a measurement of the difference between the reflectivity of Tyvek and the reflectivity of whatever material we place there, which is not very useful.
Even if we could use a perfect light absorber though, some internal backgrounds would still be unaccounted for, including those due to light being reflected from the Tyvek and then reflected into the fiber from a side of the box or, possibly, by the air-water interface when the experiment is run underwater.

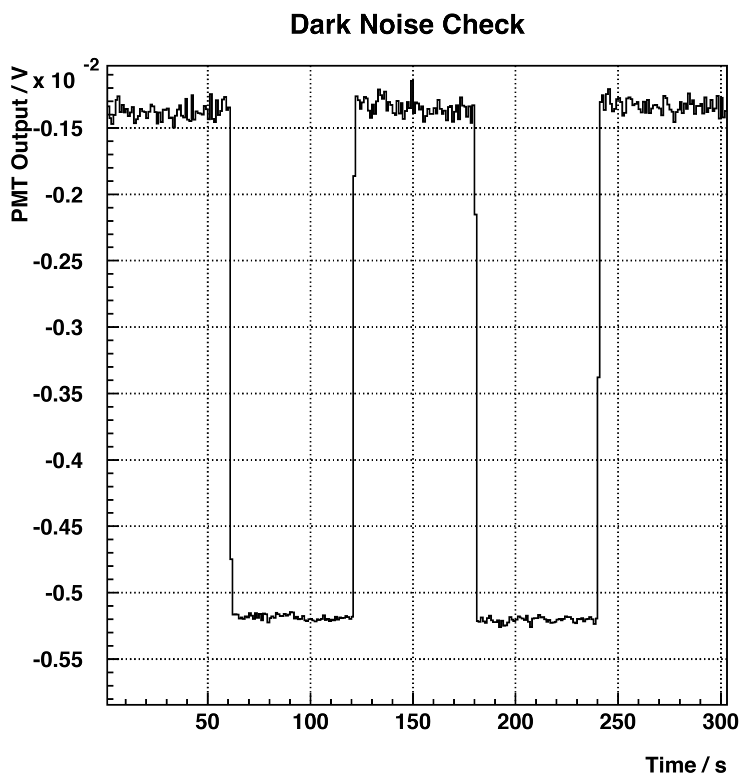

Figure 39: Plot showing how the PMT output varies when the lights in the room (external background) are turned on and off. Notice the output is 3 orders of magnitude lower than the output in the reflectivity measurement.

Given all this, we did try to minimize the internal backgrounds as much as possible by making all parts inside the box black. Still, the entire laser dot lands on the piece of Tyvek for all angles of incidence, therefore we expect the major contributions for the measured flux to be light that reflected from the Tyvek into the fiber.

4 Results

4.1 Testing the stability of the system

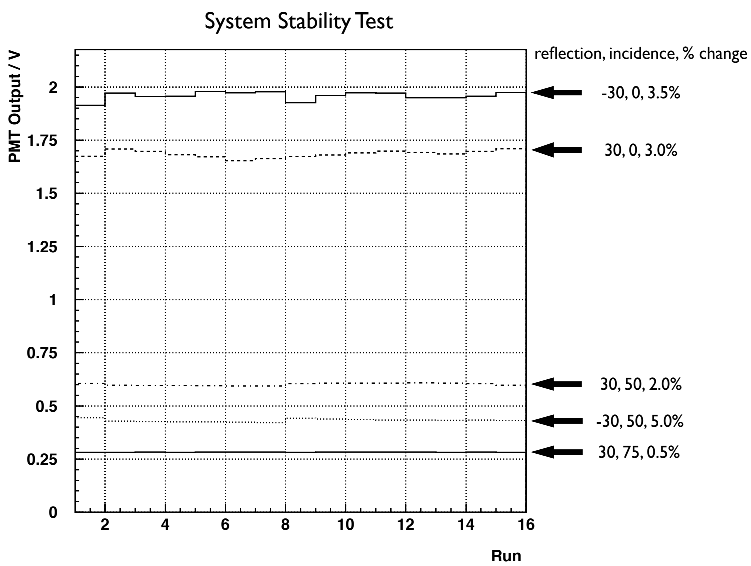

Figure 40: Results from the system stability test.

Figure 40 shows the results for this test for five of the configurations (different angles of incidence and reflection) that were tried. As it can be seen, the output does change in between runs. It is not yet understood what is the source of these jumps. Plenty of testing was done to study the nature of these jumps but no satisfactory conclusion was reached. They seem to be unpredictable and have no angular dependence. Regardless, these jumps, whose height seems to be random, represent a considerable error. This is by far the largest error in the PMT output voltage measurement and it includes the uncertainty in the output intensity of the laser. The error of the DC measurement made by LabView is very small and the error associated with the PMT output being proportional to the light intensity is also negligible (they should account for a very small part of the jumps ≈ 1 mV). Therefore, the error in the PMT output for a particular angle of incidence and reflection will be determined by looking at the error due to these jumps.

The range of values over all 15 runs for the different configurations as a percentage are shown in the next table.

Range in the PMT Output as a percentage of the average		
Angle of Incidence	Angle of reflection	Range
0	-30	3.5%
0	30	3.0%
50	-30	5.0%
50	30	2.0%
75	30	0.5%

As it can be seen, the error due to the jumps varies greatly for different angles and different trials (it might be consistent for a few runs and then, unexpectedly, it starts being unstable). It is not practical to assign this error to each angle individually and therefore we have to come up with a reasonable estimate for this error in general. Additionally, although, this error does not seem to be uniformly random (the distribution for the size of the height of the steps is considerably different between (-30°,0°) and (30°,0°)), it is still expected that for some angles that we have not tried, the error is larger than any of these. Also, not all jumps are as large as the range, so assigning the range as the error might be slightly overestimating.
Taking into consideration what has been said, it seems like a reasonable guess to take a range of 6% and assign an error for the PMT output voltage of ±3% for all measurements.

4.2 Reflectivity of Tyvek in air and water

The results for the reflectivity of Tyvek in air were collected using a PMT CV of 0.69 V, while the results for the reflectivity of Tyvek in water were collected using a PMT CV of 0.60 V. It was our intention to do both of the sets of measurements at the same control voltage (CV, which is proportional to the PMT gain), but the PMT output in water at CV=0.69 V was so large that some of the readings, especially for the larger angles of incidence, were within the saturation region, where the PMT is no longer linear. For outputs lower than the saturation range, though, the PMT output should be linear for either CV. Thus, the PMT output (outside the saturation region) that corresponds to a particular flux for CV=0.69 V should be proportional to the PMT output that corresponds to that same flux for CV=0.60 V.
To find out what this constant of proportionality is, so that we can fairly compare the results in water and air, we can compare the measurements for Tyvek in water at an angle of incidence=0° for both CV=0.60 V and CV=0.69 V (for this particular angle, the results for CV=0.69 V are still below the saturation range and, thus, still linear). Figure 41 shows these results, where the results for CV=0.60 V are scaled by a factor of 3. As it can be seen, the curves lie almost on top of each other, which implies that the PMT gain for CV=0.69 V is 3 times larger than for CV=0.60 V.

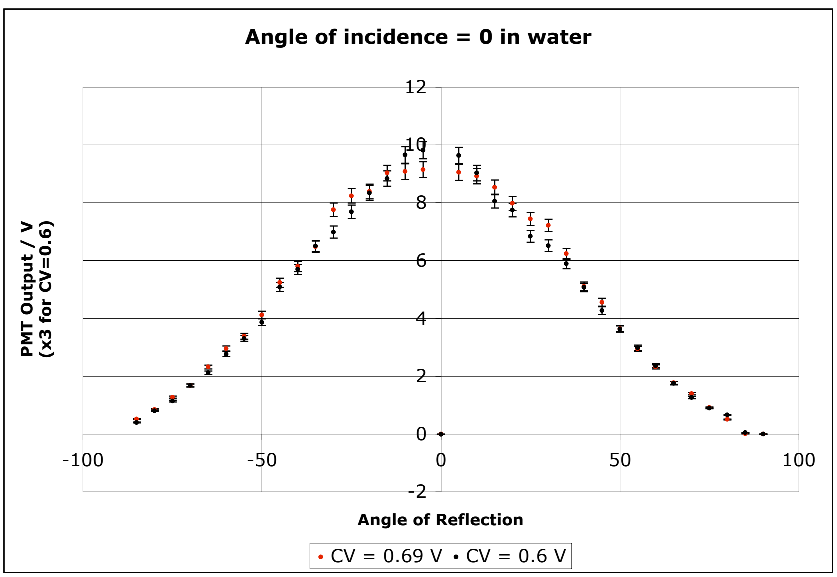

Figure 41: Graph to find out the constant of proportionality between results for CV=0.60 V and CV=0.69 V.

Thus, to accurately compare our results in water and air, we will go ahead and scale by 1/3 the results in air, which were collected with CV=0.69 V and plot them next to the results in water, which were collected with CV=0.60 V. Figures 42- 50, show the reflectivity of Tyvek on the plane of the incident laser beam. The blue markers are the results for water and the red markers are the results in air.

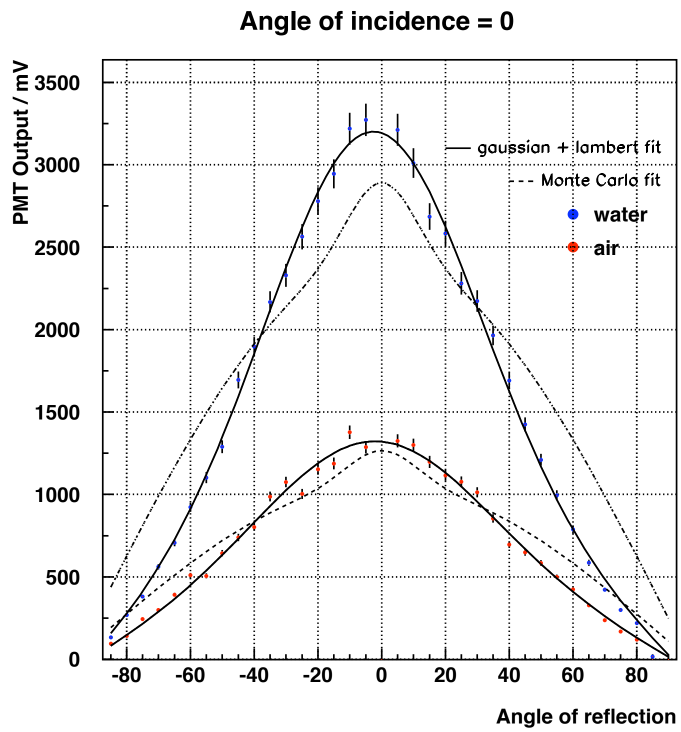

Figure 42: Reflectivity of tyvek in air (red) and in water (blue).

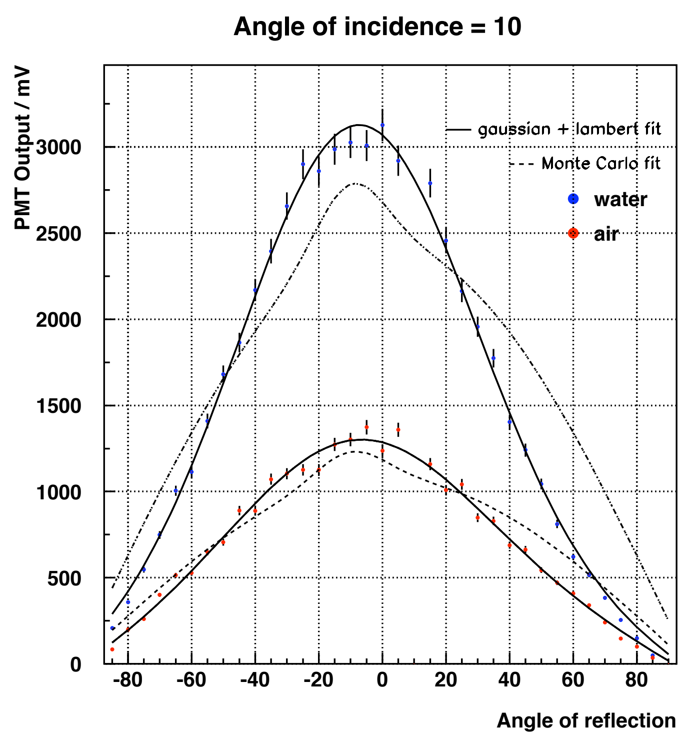

Figure 43: Reflectivity of tyvek in air (red) and in water (blue).

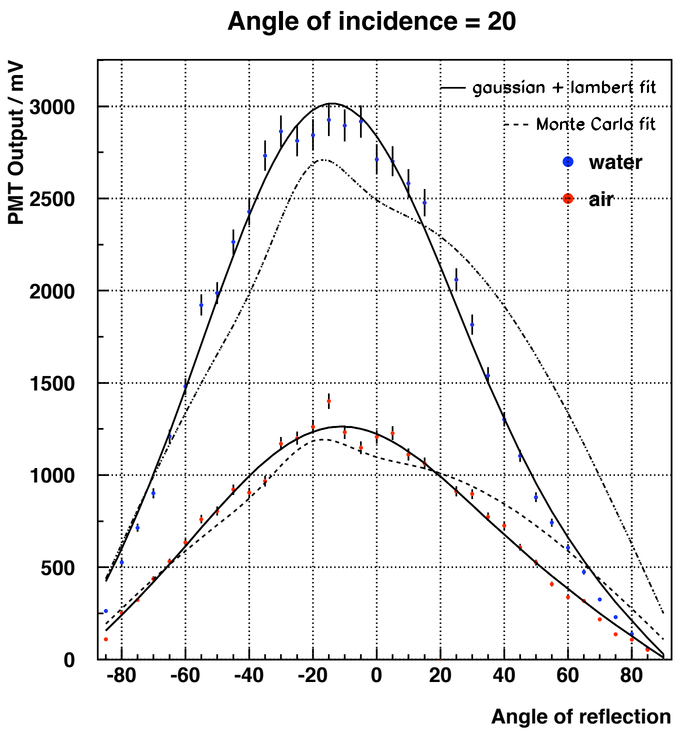

Figure 44: Reflectivity of tyvek in air (red) and in water (blue).

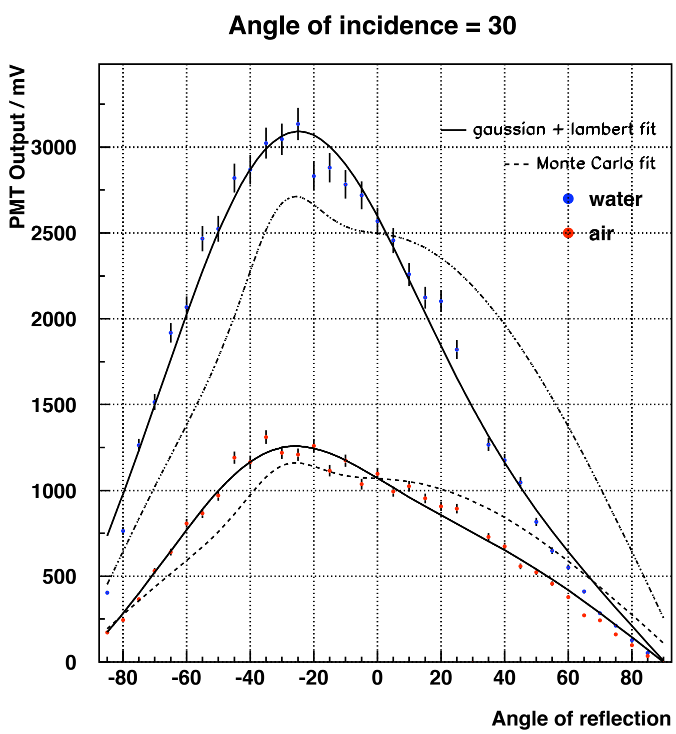

Figure 45: Reflectivity of tyvek in air (red) and in water (blue).

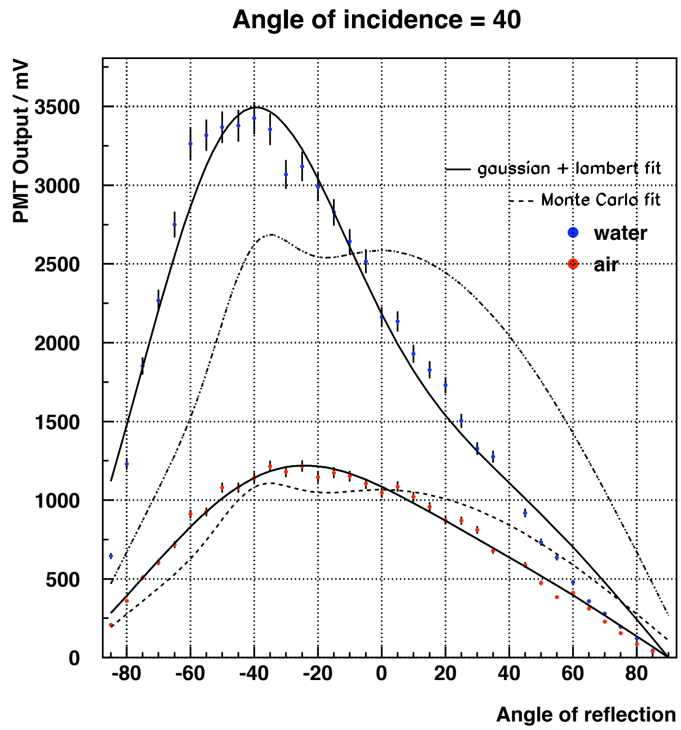

Figure 46: Reflectivity of tyvek in air (red) and in water (blue).

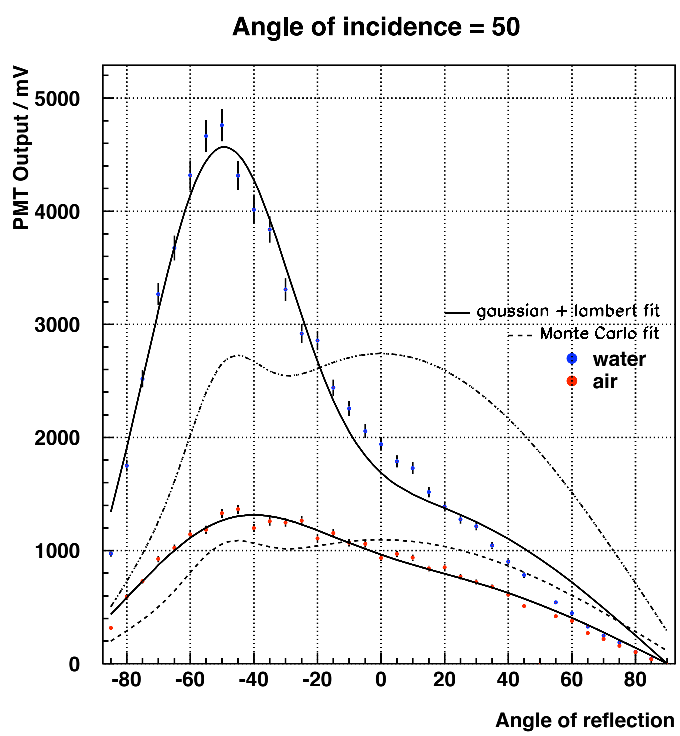

Figure 47: Reflectivity of tyvek in air (red) and in water (blue).

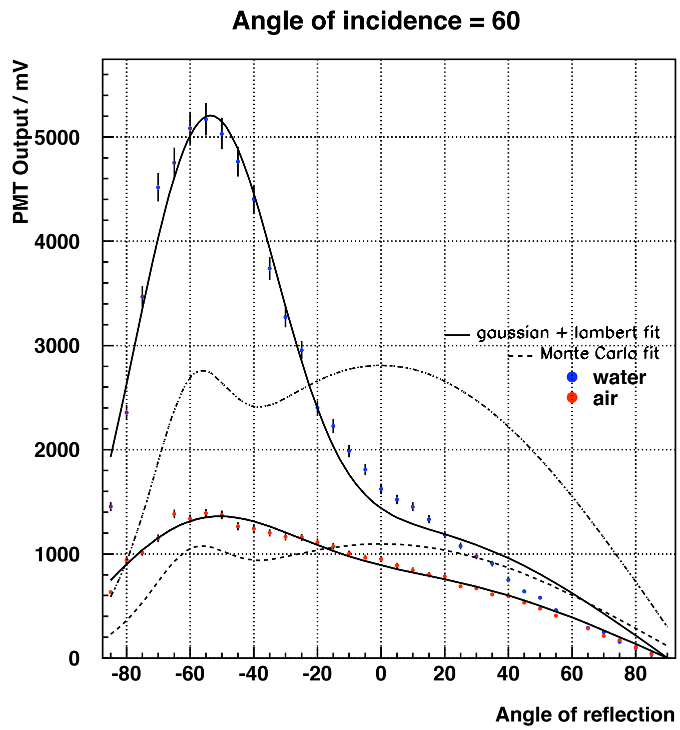

Figure 48: Reflectivity of tyvek in air (red) and in water (blue).

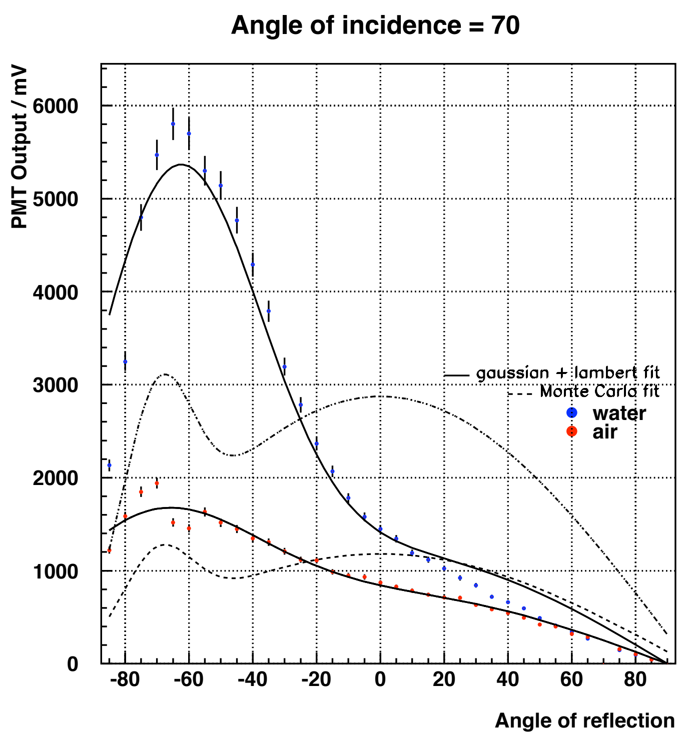

Figure 49: Reflectivity of tyvek in air (red) and in water (blue).

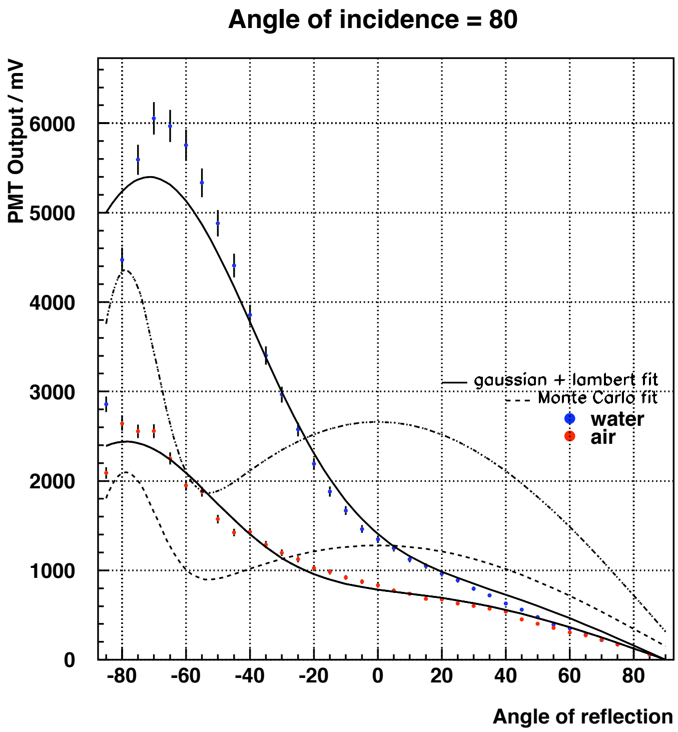

Figure 50: Reflectivity of tyvek in air (red) and in water (blue).

5 Analysis

The measured value, which is the PMT output in mV, should be proportional to the flux of the light collected by the fiber Φ and it should also be proportional to the reflected intensity, I, (flux per unit solid angle), as the face of the fiber subtends the same solid angle at all positions.

Two fits have been done to each of the set of results (Figures 42- 50) using the Physics Analysis Workstation (PAW) [13]. The first fit, f_1, which is titled “gaussian + lambert fit” in the legend of the plots and is a solid line, is of the form

$$f_1 = p_1 \cos(\theta) + p_2 e^{-\frac{(\theta - p_3)^2}{2p_4^2}} \tag{10}$$

where p_1, p_2, p_3 and p_4 are parameters to be fit by PAW. Parameters p_1, p_2 and p_4 are freely fit, while p_4 is constrained within $\theta = -\phi \pm 5$. This constraint was done because PAW had a tendency to fit the gaussian to one or two of the jumpy points, away from the peak of the function (also, because, as mentioned before, the nominal angle of reflection is 2° of the actual one). The freedom in this parameter also allows us to test if the peak of the gaussian is indeed at $\theta = -\phi$, as it was predicted in the beginning of this paper.

f_1 is then the best fit for a superposition of lambert reflection and diffused specular reflection. It is a test for the predicted function in Equation 7. The parameters for the best fits are given in the following table.

Best fit parameters for f_1					
Medium	Angle of incidence(ϕ)	p_1	p_2	p_3	p_4
air	0	574	748	-2.52	32.9
air	10	502	797	-7.58	37.0
air	20	607	671	-15.0	36.3
air	30	834	535	-35.0	27.4
air	40	768	555	-36.9	34.9
air	50	810	746	-50.8	28.6
air	60	780	924	-61.5	29.9
air	70	729	1431	-75.0	33.3
air	80	723	2347	-85.0	31.6
water	0	990	2212	-2.87	31.3
water	10	557	2575	-7.92	35.4
water	20	852	2191	-16.0	36.0
water	30	1105	2107	-29.7	35.8
water	40	1394	2459	-45	29.8
water	50	1357	3679	-51.5	22.9
water	60	1213	4490	-55.4	22.2
water	70	1158	4848	-65.0	26.6
water	80	920	5132	-75.0	34.5

The second fit that was done, f_2, which is titled “Monte Carlo fit” in the legend of the plots and is a dashed line, is of the form

$$f_2 = p_1 \left((1.13 \times 10^{-3})(1 - G(\phi)) \cos\theta + (1.21 \times 10^{-2}) G(\phi) e^{\frac{-(\theta+\phi)^2}{15^2}} + 1.27 \times 10^{-4} \right) \tag{11}$$

where there is only one parameter, p_1, which is simply a scaling factor.
This fit is Equation 9 with $F = 0.00266$ and $H = 0.00662$. These values were calculated by taking into account the size of the fiber (0.5 mm in diameter) and the distance between the face of the fiber and the center of the Tyvek ((94.0 ± 0.1) mm).

The PMT output drops to zero when $\theta = \phi$. This is because, at this point, the arm blocks the laser beam and consequently, there is no light hitting the Tyvek. These points were excluded from the fit.
In general, the output looks relatively smooth but it does get slightly jumpy near the peaks of the waveforms, especially in air. The results might look smoother in water because some of the jumpiness might be due to some vibrations of the mechanical system. Underwater, these vibrations might be damped and thus, the waveform looks smoother.
The f_1 fits look good. For the results in air, the fit seems able to get the general shape of the data curve very well for all angles of incidence. For the results in water, the fit seems to be in good agreement for angles of incidence of 0° and 10°, but as the angle of incidence goes beyond that, the fits fail to match the tail on the right-hand side of the data.
Another thing to notice is that the first few points in the tail of the functions for the results in water and air seem to match well. This is especially evident for the larger angles of incidence (ϕ) (70° and 80°), where from $\theta = 60°$ to $\theta = 90°$ the curves seem to lie on top of each other.
It is interesting to see where the parameter p_3 was fit, i.e. where the peaks of the functions lie. It is expected that, if indeed the diffused specular reflection is a gaussian centered at $\theta = -\phi$, then we would expected p_3 to be fit to this value. For $\phi = 0$ we can see that in both air and water p_3 is between $-2°$ and $-3°$. This is expected because, as mentioned earlier, the nominal angle of reflection (θ) is $\approx 2°$ off the actual value for the angle of reflection. Also, the fact that these two values are very close to each other suggests that the angle of incidence does not significantly change when the experiment is run underwater (it is possible that, if the laser beam is not incident perpendicular to the water surface, refraction might have changed the angle of incidence of the laser beam). As ϕ increases, the value for p_3 is not always close to $-\phi$. As a matter of fact, the value for p_3 for the same ϕ might be considerably different between water and air. For example, p_3 for $\phi = 70°$ and 80° is at least 10° greater in air than in

water. One reason why p_3 does not have the expected value might be the fact that the diffused specular peak, that has been approximated with a gaussian, is not symmetric. By looking at the left-hand side of the plot, it can be seen that, for $\phi > 10^\circ$, the fit, for either water or air, never drops close to zero at $\theta = -90^\circ$, as it should. Furthermore, the bad fits for large ϕ in water can be blamed on the fact that the gaussian decreases much faster than the data points, causing the fit to compensate by increasing the cosine contribution, thus why many points in the tail are missed. It might be better to find a function that has a predominant peak, like a gaussian, but is asymmetric enough such that one side of the peak falls much more quickly than the other. Additionally, there are no theoretical reasons to believe that the peak should be exactly at the angle of specular reflection, only near it, therefore, as long as the peak is relatively close to $-\phi$ (as it is the case in all results), there is no reason to doubt the quality of the data.

The total flux detected on the slice of the hemisphere that we are probing (i.e. $\approx$ the plane of the incident light beam) should be proportional to

$$\Phi_t(\phi) \propto \int_{\frac{-\pi}{2}}^{\frac{\pi}{2}} V(\theta, \phi) d\theta \tag{12}$$

$$\Phi_t(\phi) \propto \int_{\frac{-\pi}{2}}^{\frac{\pi}{2}} C_1 e^{-(\theta+\phi)^2/s} d\theta + \int_{\frac{-\pi}{2}}^{\frac{\pi}{2}} C_2 \cos\theta d\theta \tag{13}$$

$$\Phi_t(\phi) = \Phi_S(\phi) + \Phi_L(\phi) \tag{14}$$

where ϕ is the angle of incidence, θ is the angle of reflection (both on the plane of the incident beam), $V(\theta, \phi)$ is the PMT output at a particular angular position, $\Phi_S(\phi)$ is the component of $\Phi_t(\phi)$ due to diffused specular reflection and $\Phi_L(\phi)$ is the component of $\Phi_t(\phi)$ due to lambertian reflection.
It is possible to introduce the ratio $\frac{\Phi_t(\phi) \text{ in water}}{\Phi_t(\phi) \text{ in air}}$. This value represents, for a particular angle of incidence, how much more likely it is for a photon to reflect into the plane of the incident direction in water than in air. These values were obtained by doing the integration in Equation 13 with the fit parameters that were returned by PAW. The results are shown in the table below.

Ratio of reflectivity in water/air	
Angle of incidence (ϕ)	$\frac{\Phi_t(\phi) \text{ in water}}{\Phi_t(\phi) \text{ in air}}$
0	2.25
10	2.22
20	2.25
30	2.33
40	2.48
50	2.52
60	2.55
70	2.44
80	2.14

These results shed some light into the very evident fact (from the plots) that, at least in the plane of the incident light, Tyvek in water seems to be much more reflective than Tyvek in air. By looking at the results in the previous table, we can see that for all values of ϕ we get between 2.0 and 2.5 more photons collected by Tyvek in water than in air. This is somewhat surprising as in air, Tyvek is already highly reflective, with an absolute reflectivity of $\approx 90\%$. Thus, although it is impossible to get, overall, twice as many photons being reflected from Tyvek in air than in water, it could be possible that given the different refractive index of the media (air=1, water=1.33, polyethylene=1.5), the light reflected by Tyvek in water is more concentrated about the plane of the incident beam.

Given that we can only compare the waveforms for different ϕ in shape and not in absolute values, it is useful to introduce the ratio $\frac{\Phi_S(\phi)}{\Phi_L(\phi)}$. This number represents, for a particular angle of incidence (in either air or water), how much more likely it is for a photon to be reflected in a diffused specular fashion than in a lambertian fashion, *if* it is reflected into the plane of the incident direction. The values for the two terms of the integrand in Equation 13 were computed using the fit parameters returned by PAW. The ratio between these two integrands should be $\frac{\Phi_S(\phi)}{\Phi_L(\phi)}$. The results, for all angles of incidence in air and water, are shown below.

Ratio of gaussian/cosine components		
Angle of incidence (ϕ)	$\frac{\Phi_S(\phi)}{\Phi_L(\phi)}$	
	Air	Water
0	0.931	1.52
10	1.26	3.53
20	0.859	1.98
30	0.375	1.42
40	0.517	1.07
50	0.527	1.30
60	0.643	1.690
70	0.963	2.02
80	1.26	2.81

For large ϕ (70° to 80°), in both air and water, the fraction of the photons that are reflected in a gaussian way is large. For $\phi = 30°$ to 60° the ratio of the photons that are reflected in a lambertian way is largest. The smallest values of ϕ also have considerable large gaussian components, especially $\phi = 10°$, which seems to be the most gaussian of them, in both air and water.

As it can be seen from the table and the plots, in general, the results in water have a larger diffused specular component than the ones in air (results in air are predominantly lambertian ($\frac{\Phi_S(\phi)}{\Phi_L(\phi)} < 1$), while results in water are predominantly diffused specular ($\frac{\Phi_S(\phi)}{\Phi_L(\phi)} > 1$). This is consistent with the fact that more light is reflected in the plane of the incident light in water. The lambertian component is expected to be uniformly spread out over the entire hemisphere, while the diffused specular component is expected to be preferential about the plane of the incident light. Thus, if water reflects a larger fraction of the photons in a diffused specular fashion then it is expected for more photons to be reflected into the plane of the incident light, as it is observed. Still, we do not know by what factor this increase should be.

The Monte Carlo fit (dashed) is closer to the results in air than in water. Still, even for the results in air, it seems that the lambertian component in the Monte Carlo is too large. As ϕ increases and the gaussian component of the data increases, the Monte Carlo fit gets much worse. For $\phi > 50°$ in air, the Monte Carlo seems to miss the predominant peak at the angle of specular reflection, and instead it has a large hump due to the cosine function that does not exist in the data. For the results in water, which have a larger gaussian component than the results in air, the Monte Carlo fit fails to agree well with the data for any ϕ.

The spread of the gaussian (s) for the function in the Monte Carlo is $s = 15°$. For the best f_1 fits, the parameter p_4, which is related to the spread by $\sqrt{2}p_4 = s$ is consistently around 30° ($s = 42°$). This means that the spread of the gaussian in the Monte Carlo is too small, with a more realistic value being three times as much as it currently is (although, eventually s could be made dependent of ϕ for a more accurate simulation).

Also, from the data, we can see no evidence for the existence of a uniform (isotropic) component in the reflective properties of Tyvek.

6 Discussion

The main doubt we have about these results is the large difference there is between the measured reflectivity of Tyvek in water and in air. We are very confident about the results in air because they do not only agree very well with expectations, but there are no reasons to doubt them. The alignment was done properly and checked multiple times and there are no sources of internal backgrounds that could cause a large difference in the data.

On the other hand there is one reason to doubt the accuracy of the results in water. This is the internal background due to reflection of light from the water-air interface. The water level is ≈ 1 cm above the location of the fiber. Taking into account the distance between the face of the fiber and the Tyvek (≈ 9.5 cm), it is evident that there will be an image of the dot on the Tyvek at an angular position of $\approx 10^\circ$ above the face of the fiber. We do not expect the fiber to accept much light that is incident on it at this large angle, but this is a possibility. If some of this light is detected, then it may partially account for the fact that Tyvek appears to be more reflective in water than air. If this is the case, though, then the image would be present at all angles of incidence and reflection and thus, what we measure is a superposition between the reflectivity function on the plane of the incident light (for a particular θ and ϕ) and the reflectivity function 10° above the plane of the incident light (for the same θ and ϕ). A problem with this hypothesis, though, is that, given that we expect reflectivity functions away from the plane of the incident light to have a larger lambertian component, then, if this hypothesis is correct, the measured flux should have a larger lambertian component than it is expected; yet, from the results in water, we can see that it is the gaussian component the one that is unexpectedly large and contributes the most to the measured flux! Laser light that is bouncing around in the box is not a considerable source of internal backgrounds, as we would expect this background to be relatively isotropic and cause significant PMT readings when the fiber is not pointing to the Tyvek and this is not the case. Some more experimentation is necessary to confirm the results in water.

As it has been mentioned, the diffused specular component of the data does not seem to be symmetric and, therefore, a gaussian fit may not be the best approximation. It is necessary for the fitting function to have a well defined peak, but it would be preferable to have a function that has a very sharp drop on one side of the peak and a gentler tail on the other side. A function of this form might improve the fits in water for $\phi > 40^\circ$, where the gaussian seems to decrease too rapidly to properly account for the tail.

Also, a way has to be devised to normalize the results. It is necessary to figure out from what part of the laser dot the fiber is collecting light and what is the irradiance (flux per unit area) on the Tyvek over this part of the dot. An improvement for the experiment that has been proposed might help for this.

The idea is to install the piece of fiber at the end of a long black tube that has the same width as the fiber (1 mm). If the tube is long enough such that the face of the fiber is 5 cm into it, then the sides of the tube will block all the light except that which comes from an angular displacement of $\pm 0.5^\circ$ about the normal to the face of the fiber. This will not only block most backgrounds (including the image due to the air-water interface discussed above) but it will define what area of the Tyvek the fiber "sees". Thus, by assuming the fiber collects all the light over this $\pm 0.5^\circ$ range (a good approximation), and by knowing what is the irradiance of the laser on the area of the Tyvek seen by the fiber, it is possible to normalize the results.

Besides this major improvement, some minor changes can be done to try to improve the overall quality of the results. The jumpiness of the results, which is especially noticeable at the peaks of the reflectivity functions in air, may be further studied. If this is due to some vibrations, it might be a good idea to try to use some vibration isolation material on the bottom of the box. Also, given that the jumpiness is relatively random, it might be reasonable to collect many runs of data and pick the ones that have the least jumpiness (some quantifiable jumpiness criteria might be developed for this).

Additionally, data can be collected at a much higher resolution. The presented data in this paper is in steps of 10° for ϕ and 5° for θ, yet the minimum step size of the rotation stages is $1^\circ/400$. Thus, given sufficient time and patience, data may be recorded in steps of 1° or smaller.

It would also be interesting to check to see if there are any variations on the reflective properties of different pieces of Tyvek. In this experiment only one piece of Tyvek was used, but a larger study, with more samples of Tyvek could be carried out.

Finally, the current setup can be further expanded to study the reflectivity of Tyvek at different wavelengths of incident light. We are particularly interested in Cherenkov radiation, whose spectrum peaks at a shorter wavelength than the green laser that is currently in use. Some new light sources might be acquired and adapted to work in the current setup. After this, the reflective properties of Tyvek can be measured at higher frequentcies to even further improve the Super-Kamiokande Monte Carlo simulation.

7 Conclusion

In this experiment, the reflectivity of Tyvek was measured in air and in water. It was found that the results in air fit very well the expected function, which is a combination of Lambert's Cosine Law (due to highly diffusive reflection) and a diffusive specular component that still retains some angular dependence (Equation 7). The results in water also agree well with the fits for $\phi < 40^\circ$, while at larger angles of incidence the fit seems to miss the tail of the data.

The reflectivity of Tyvek in the plane of the incident light seems to be much larger in water than in air (by a factor of 2.0-2.5 depending on the angle of incidence). This is consistent with the fact that, in water, the reflectivity functions appear to have a predominant diffused specular component, which reflects photons preferentially about the plane of the incident light. Yet, we cannot tell if this is sufficient to account for this large difference.

It was realized that there might be better functions to model the diffused specular component than a gaussian. The peak of the reflectivity data does not seem to be symmetric; it appears to have a sharp decay in one side and a smooth tail in the other. This asymmetry appears to be the reason why the fit to the expected function is not very good for $\phi > 40^\circ$ in water.

The implementation of the reflection of photons from Tyvek in the Monte Carlo simulation can be greatly improved using the fits for the results in air and water. It has been stated that it is unrealistic to have all the photons that are reflected in a diffused specular way to be reflected on the plane of the incident light and thus, a simple correction (i.e. distributing the photons $\pm 30^\circ$ above and below this plane) has been introduced to fairly compare the data to the current Monte Carlo. It was found that even though the Monte Carlo results look reasonable for low values of ϕ in air, they fail to agree with the results for large ϕ in air and with all the results in water. This is because, in the Monte Carlo, the gaussian component is too small and it does not dominate at large ϕ, as it is suggested by the data. Additionally, the width (s) of the gaussian distribution used to model diffused specular reflection in the Monte Carlo is too small ($s = 15^\circ$). It was found for all of the results in water and air that s for the gaussian component was always $\approx 40^\circ$, about 2-3 times as large as the value in the simulation.

References

[1] The Superkamiokande Detector, The Super Kamiokande Collaboration, Nucl. Instrum. Meth. A501(2003)418-462, 2002

[2] Photo Album of Super-Kamiokande, Institute of Cosmic Ray Research, University of Tokyo, http://www-sk.icrr.u-tokyo.ac.jp/sk/index-e.html

[3] What is Tyvek?, DuPont, http://www.tyvek.com/whatistyvek.htm

[4] A study on the transmittivity of Tyvek, Alvaro Chavarria, http://www.phy.duke.edu/ aec19/trans .pdf

[5] Specific Technical Questions - Standards and TIPs, TAPPI, http://www.tappi.org/

[6] Photographie 22 : surface d'un non-tisse Tyvek, Ecole Francaise de Papeterie et des industries Graphiques, http://cerig.efpg.inpg.fr/tutoriel/non-tisse/photo22.htm

[7] Product Handbook for DuPont Tyvek, DuPont, http://www.tyvek.com/pdf/prod_techman.pdf

[8] Tyvek diffuse reflectivity, Hasenbalg, F., Ravignani, D., Department of Physics, TANDAR Laboratory, C.N.E.A., Buenos Aires, Argentina, 1997

[9] Spectral-directional reflectivity of Tyvek immersed in water, Filevich, A., Bauleo, P., et al., CNEA, Buenos Aires, Argentina

[10] SKIII Tyvek Fest, Christopher Walter, http://www.phy.duke.edu/ cwalter/photos/SKIII/

[11] Principles of Optics, Born, M., Wolf, E., Pergamon Press Inc., New York

[12] LabView, National Instruments, http://www.ni.com/labview/

[13] Physics Analysis Workstation, CERN, http://paw.web.cern.ch/paw/